Chapter 7

# Enhancing the Light Harvesting Capacity of the Photoanode Films in Dye-Sensitized Solar Cells

Xiang-Dong Gao, Xiao-Min Li and Xiao-Yan Gan

Additional information is available at the end of the chapter

http://dx.doi.org/10.5772/51633

## 1. Introduction

Dye-sensitized solar cell (DSC) has been receiving continuous academic and industrial attention as a potential low-cost, clean, and renewable energy source, since its inception in 1985 (Desilvestro et al., 1988; Regan et al., 1991; Gao et al., 2008; Hagfeldt et al., 2010; Yella et al., 2011). The DSC is the only photovoltaic device that uses molecules to absorb photons and converts them to electric charges without the need of intermolecular transport of electronic excitation. It is also the only photovoltaic device that separates two functions of light harvesting and charge-carrier transport, mimicking the photosynthesis found in green leaves. The primary photon-to-electron conversion process in DSC occurs at the oxide/dye/electrolyte interface, functioning at a molecular and nano scale. There exist many complicated optical, electrical, and chemical processes during the light-to-electric conversion process in DSC, including the light absorption of dye molecules (producing electrons and leaving the dyes in their oxidized states), the electron injection from dyes to the conduction band of semiconductor (e.g., $TiO_2$), the percolation of electrons through the mesoporous semiconductor network toward the bottom electrode, the recombination of photo-excited electrons in the porous electrode with either oxidized dyes or acceptors in the electrolyte, and the regeneration of dye molecules by iodides in the electrolyte etc. For an efficient DSC device, while above processes should be kept in a complicated and delicate balance, the high light-harvesting, the rapid electron transport, and the minimum electron-hole recombination are essential. In special, the light-harvesting efficiency of the photoanode is the most important and indispensable factor for the high-efficiency DSC, which is mainly related to the molar extinction coefficient of the sensitizer, the dye-loading capacity of the porous electrode, and the optical path of the incident light in the electrode.

At present, the record efficiency of DSC has reached 12.03% (Yella et al., 2011) after the first breakthrough of M. Grätzel in 1991 and through the continuous efforts of the scientists for more than 20 years. With an aim to further improve the conversion efficiency of DSC to 15% or higher, recently, intensive efforts have been directed to enhance the functions of the major components in DSC, focusing on mainly three aspects, i.e., the ordered nanoporous electrode, the novel organic or quantum-dot sensitizer, and the new redox electrolyte system (Hagfeldt et al., 2010; Tetreault et al., 2012). During this journey toward high-efficiency DSC, the light-harvesting capacity of the photoanode is expected to play a critical and indispensable role by spanning the mesoporous electrodes utilizing varied nano/meso materials and the sensitizers with high molar extinction coefficient or quantum dots, and by connecting the optical functions of the photoanode with its electrical response together.

There are mainly two components concerning the light-harvesting property of DSC, the dye and the mesoporous electrode which supports the sensitizer. While the development of the novel sensitizers with higher molar extinction coefficient and better response to near-infrared wavelength has been long studied since the first breakthrough of DSC in 1991 (Nazeeruddin et al., 2001; Grtäzel et al., 2009; Yum et al., 2011), the significance of the light scattering and/or reflection of the mesoporous electrode on the light-harvesting properties is only recognized in recent years. Accompanying the rapid advance of the ordered or hybrid photoanode materials, novel semiconductor nanostructures or new concepts are widely used to construct new type photoanodes, including the plenary optical waveguide nanowire enhancing the multiple internal reflections (Wei et al., 2010), the plasmonic core-shell metal-insulator nanoparticles enhancing the near-infrared absorption (Brown et al., 2011), the dual-function mesoporous $TiO_2$ structures increasing both the dye-loading and the optical scattering effects (Koo et al, 2008; Huang et al., 2010), and so on. In view of the wide coverage of the optical and photoelectrical nanostructures involved in these studies and their rapid progresses, it is great valuable to make a comprehensive and in-depth review on the current status of the light-harvesting capacities of the photoanode in DSC.

The chapter will start with a brief description of the basic concept of the light-harvesting efficiency (LHE), and then give a review on five typical branches representing the significant advances in this area, including

1. the mesoporous photoanodes with high surface area,
2. the hierarchically nanostructured photoanodes,
3. the dual-function scattering layer on the top of nanocrystalline (nc) electrode,
4. the plasmonic photoanodes, and
5. the photonic crystal photoanode and others.

The basic principles of these novel nanostructures/ methods enhancing the light-harvesting capacity of DSC, together with their mutual effects on the electrical and photoelectrochemical properties of the nanoporous electrode, will be discussed in detail. Based on the in-depth analysis of literature and the authors' experience, a perspective will be presented, shedding a light on the research road in near future.

http://dx.doi.org/10.5772/51633

## 2. The Light Harvesting Efficiency (LHE)

The typical DSC device is a sandwich type electrochemical cell, as seen from Figure 1, with the dye molecules absorbing the incident sunlight, and the framework of $TiO_2$ mesoporous electrode transporting the photo-excited electrons generated from dye molecules to the bottom electrode. Therefore, the semiconductor porous electrode, or the photoanode film, is the kernel component in DSC, undertaking two major functions: supporting dye molecules, and transporting photo-excited electrons. To harvest the sunlight as far as possible, the photoanode film has to possess a high internal surface area, to guarantee the massive uptake of dye molecules. The cell performance of DSC, that is, the solar-to-electric conversion efficiency, is determined by the short-circuit photocurrent ($J_{sc}$), open-circuit photovoltage ($V_{oc}$), and fill factor (*FF*) under a definite intensity of light such as the AM 1.5 solar spectrum. $J_{sc}$, the critical parameter affecting the power conversion efficiency (PCE) of DSC most, can be increased by raising the light-harvesting efficiency (LHE), which is defined by Equation 1,

$$\mathrm{LHE}\,(\lambda) = 1 - 10^{-\Gamma\sigma(\lambda)} \tag{1}$$

where Γ is the number of moles of sensitizer per square centimeter of projected surface area of the film, and σ is the absorption cross section in units of $cm^2$/mol obtained from the decadic extinction coefficient (units of $M^{-1}$ $cm^{-1}$) by multiplication with 1000 $cm^3$/L (Nazeeruddin et al., 1993). The LHE is directly determined by the surface concentration of the dyes in the film, and the molar extinction coefficient of dye. The LHE, together with the quantum yield of charge injection ($\varphi_{inj}$) and the efficiency of collecting the injected charge at the back contact ($\eta_c$), determines the incident monochromatic photon-to-current conversion efficiency (IPCE), defined as the number of electrons generated by light in the external circuit divided by the number of incident photons (Equation 2).

$$\mathrm{IPCE}\,(\lambda) = \mathrm{LHE}\,(\lambda)\varphi_{inj}\eta_c \tag{2}$$

Previous studies proved that $\varphi_{inj}$ is a wavelength independent parameter, and almost all of photons absorbed by the sensitizer are quantitatively converted to the conduction band electrons (Nazeeruddin et al., 1993). Meanwhile, the time-resolved laser photolysis experiments showed that the injected electrons can percolate without significant loss through the network of interconnected particles present in the nc-$TiO_2$ film, and the back reaction is relatively slow, indicating that the majority of the injected charges is able to reach the back contact, and the influence of $\eta_c$ on IPCE is minor (Regan et al., 1990). So the wavelength-depedent LHE has predominant effects on the IPCE and the PCE of DSC.

In essence, the LHE of DSC is the electrical response of the photovoltaic device to the solar spectrum projected on earth. It is predominantly related to there factors, the wavelength dependent light-absorbing capacity of the dye molecules, the quantity of the dye molecules adsorbed on the porous electrode, and the optical path of the incident light traveled in the

electrode (determining the collision numbers of the light with the dye molecules). As a wavelength-dependent parameter, the LHE is usually evaluated by the IPCE spectrum. Figure 2 gives the IPCE spectrum of a typical DSC with nc-$TiO_2$ electrode, N719 dye and $I_2/I_3^-$ electrolyte system, and its comparison with the standard solar irradiation spectrum (ASTM G173). To characterize the response of DSC to the solar irradiation, the IPCE spectrum can be divided into four wavelength zones, i.e., the strong absorption zone between 500-550 nm, two moderate absorption zones between 400-500 nm and 550-700 nm, and the weak absorption zone above 700 nm. While the broadband or near-infrared absorption sensitizers are devised to harvest the sun light beyond 700 nm, the modulation of the optical path of the incident light by introducing scattering or reflection is mostly used to improve the light harvesting in two moderate absorption zones. From the viewpoint of the photoanode film (i.e., the porous electrode), there are several measures to improve the LHE, including

1. increasing the internal surface area of the electrode, which has the potential to improve the dye-loading capacity of the photoanode over a specific film thickness and area;
2. increasing the optical path of the incident light in the electrode, by introducing scattering centers in the bulk film, by introducing the scattering layer on the top of nanocrystalline electrode, and by constructing hierarchical structures possessing strong light scattering effects; and
3. enhancing the absorption of dye molecules by introducing plasmonic metal-semiconductor structures.

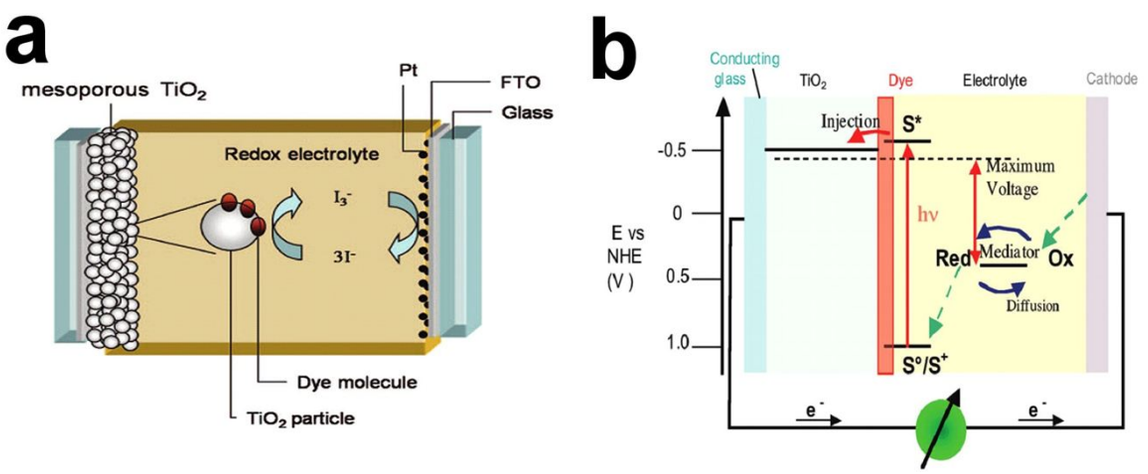


**Figure 1.** a) Schematic illustration of dye-sensitized solar cells (Hagfeldt, et al., 2010). b) Working principle of a typical DSC employing an iodide/triiodide-based redox electrolyte and N719 as a sensitizer (Grätzel, 2009).

In current days, the nanocrystallite electrode is confronting the maximum photocurrent theoretically achievable with the Ru-based sensitizers (e.g. N719 dye), and the quest for the novel nanostructured photoanode has becoming prosperous (Zhang et al., 2011; Tetreault et al., 2012). Among numerous innovative nanostructured photoanodes, a considerable amount of studies are directed to improve the LHE of the photoanode, in view of the moderate surface

http://dx.doi.org/10.5772/51633

area, the moderate electron transporting property of nc-$TiO_2$ electrode, and the intrinsically low-surface-area nature of the traditional submicron scattering layer. In the following sections, we will introduce five typical research branches in this area, to provide readers with a comprehensive and in-depth overview on the development of the LHE studies in DSC.

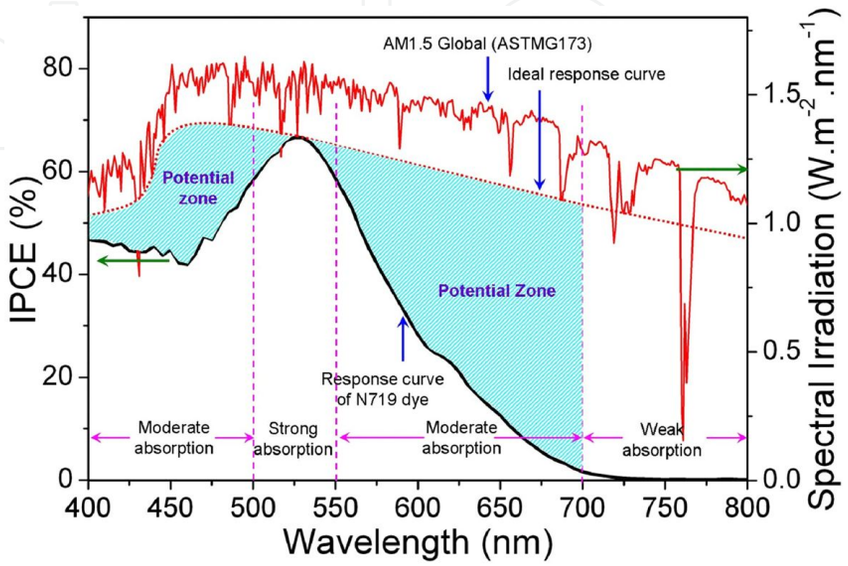


**Figure 2.** The light-harvesting capacity of N719 sensitized nc-$TiO_2$ photoanode in DSC and its comparison with AM 1.5 Global solar spectrum.

## 3. Mesoporous photoanodes with high surface area

It is essential for the photoanode in DSC to possess a high internal surface area, to adsorb sensitizer as much as possible. Typically, the hydrothermal nc-$TiO_2$ with the particle size of 15-30 nm is used to fabricate the porous electrode, which usually exhibits the BET surface area of 50-100 $m^2/g$. While these nanocrystallite photoanodes perform fairly well and occupy the highland of DSC with the best efficiency, their moderate dye-loading capacity motivate researchers to seek other materials with higher surface area. In fact, there are several materials which do possess much higher surface area than nc-$TiO_2$ electrode, such as the mesoporous materials, aerogel, and metal-organic framework (MOF), whose surface area usually range from several hundred to three thousand $m^2/g$. It is greatly intriguing to construct photoanodes using these high-surface-area materials, which is expected to remarkably improve the dye-loading capacity of the photoanode and the PCE of DSC in case a good charge transport can be maintained in these mesoporous structures. Up to date, mesoporous $TiO_2$ in the form of powder, sphere, bead, or film, and aerogel have been used to synthesize the photoanode, which usually exhibited the surface area of 100-1100 $m^2/g$. Here we present some typical mesoporous photoanodes prepared by the high-surface-area $TiO_2$ mesostructures and $TiO_2$ aerogel.

Mesoporous powders possessing a large volume of mesopores and irregular micron/ submicron secondary particles are the mostly-used materials in constructing the mesoporous photoanodes. The template methods are the common strategy to prepare these mesoporous powders. For example, T. K. Yun et al. prepared two different mesoporous $TiO_2$ powders, using a soft template of tri-block copolymer and a hard template of mesoporous ZnO/ $Zn(OH)_2$-composite, respectively (Yun et al., 2011). Both mesoporous $TiO_2$ possessed the same high surface area (BET ~210 $m^2/g$) but with different pore sizes of 6.8 (for soft template) and 3.0 nm (for hard template). Different photovoltaic performances were observed. While the photoanode using the mesoporous $TiO_2$ having larger pores showed the PCE of 6.71%, higher than P25 $TiO_2$ nanopowders based photoanode ($\eta$= 5.62%), only half the performance (3.05%) was observed for the mesoporous $TiO_2$ having small pores. The work indicated that, a suitable selection of the pore sizes was important for mesoporous materials used in DSC, and a too small pore size would inhibit the diffusion of dye molecules through the pores, thus greatly reducing the uptake of the dye molecules.

Beside the template method, the external fields such as the microwave irradiation can also be very useful in synthesizing mesoporous $TiO_2$ powders. C. H. Huang et al. reported the rapid synthesis of mesoporous $TiO_2$ via a microwave-assisted hydrothermal route using water-soluble titanium citrate complexes as the precursor, and obtained $TiO_2$ powders showed the surface area of 217–323 $m^2/g$, and the pore diameter of 5.8–6.9 nm (Huang et al., 2011). The photoanode based on this mesoporous $TiO_2$ exhibited the highest conversion efficiency of 7.1% (active area: 0.25 $cm^2$). Also, the cell exhibited good long-term stability, and the PCE of a 1 $cm^2$ device decreased merely from 4.8% to 4.3% after being stored for more than 490 h.

For most photoanodes using the high-surface-area mesoporous materials, it is required to prepare the mesoporous powders first, and the final electrode is obtained via the doctor-blade method using the mesoporous paste prepared from the mesoporous powders. This is a relatively complicated process. In contrast, W. Chen et al. developed a facile one-step preparation of crack-free thick ordered mesoporous $TiO_2$ films, via the combination of ''doctor blade'' technique and the evaporation induced self-assembly method (Chen et al., 2007). By employing the as-synthesized mesoporous film (7 μm in thickness) as the photoanode, a PCE of 6.53% was obtained at 30 $mW/cm^2$ light intensity, illustrating the potential of this simple strategy in constructing powerful DSC devices.

While the mesoporous materials of pure $TiO_2$ give a promising potential to improve the LHE, the introduction of other oxides (e.g., $Al_2O_3$, $SiO_2$) in the mesoporous structure of $TiO_2$ opens an alternative route to enhance the LHE of DSC. As an example, J. Y. Kim et al. prepared highly ordered mesoporous $Al_2O_3/TiO_2$ via a sol-gel reaction and evaporation-induced self-assembly route using Pluronic P123 as the structure-modifying reagent (Kim et al., 2011). Obtained mesoporous powders possessed an average pore size of 6.33-6.58 nm, and BET surface area of 181-212 $m^2/g$, and the content of $Al_2O_3$ had significant effects on the BET surface area. The thin $Al_2O_3$ layer was located mostly on the surface of mesopore (as seen in X-ray photoelectron spectroscopy (XPS) spectra in Figure 4c), blocking the charge recombination during the photon-to-electron conversion process. The photoanode based on the mesoporous $Al_2O_3/TiO_2$ (1 mol % $Al_2O_3$) exhibited ~10% efficiency improvement com-

http://dx.doi.org/10.5772/51633

pared to the pure mesoporous $TiO_2$ electrode ($\eta$ increasing from 5.88% to 6.50%). Though the authors didn't compare their results with traditional nanocrystalline counterpart, the much higher surface area of the mesoporous electrode than P25 $TiO_2$ may possibly lead to higher dye-loading quantity, and corresponding higher light-harvesting capacity. Also, the introduction of $Al_2O_3$ barrier layer in mesoporous $TiO_2$ illustrated a viable and versatile route to further improve the functions of the mesoporous photoanodes.

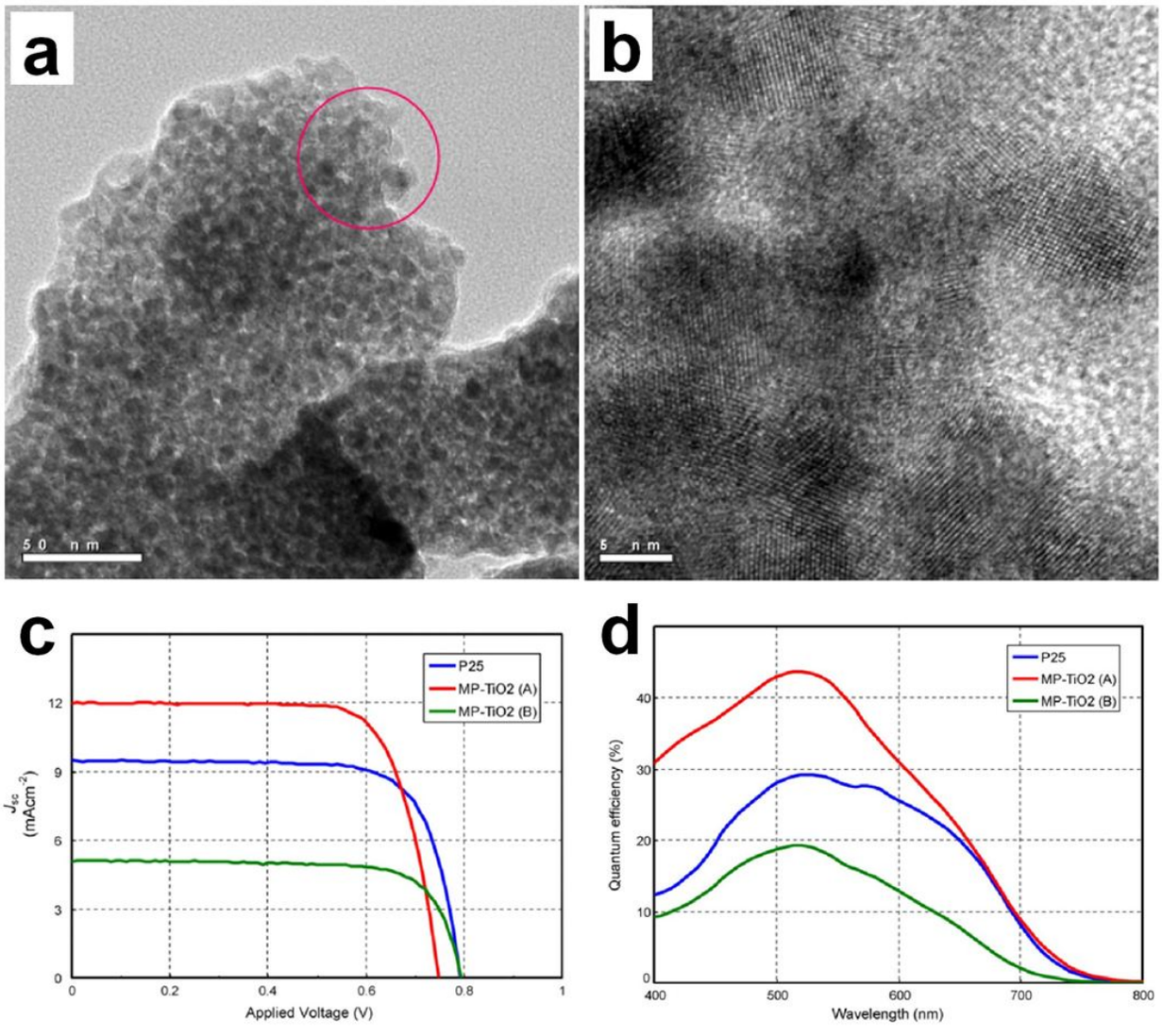


**Figure 3.** TEM image of mesoporous $TiO_2$ with a) low and b) high magnifications. c) *J*-V curves and d) IPCE spectra of DSCs prepared from P25 and mesoporous $TiO_2$ with $TiCl_4$ post-treatment. (Yun et al., 2011).

Though above mesoporous powders with irregular secondary particles are promising in improving the dye-loading capacity of the photoanode, it is usually difficult for them to obtain high quality electrodes with good transparency, due to the poor workability of the paste produced from the irregular micron/submicron particles. Therefore, it is intriguing to prepare mesoporous $TiO_2$ with regular secondary particles, e.g., $TiO_2$ mesoporous spheres.

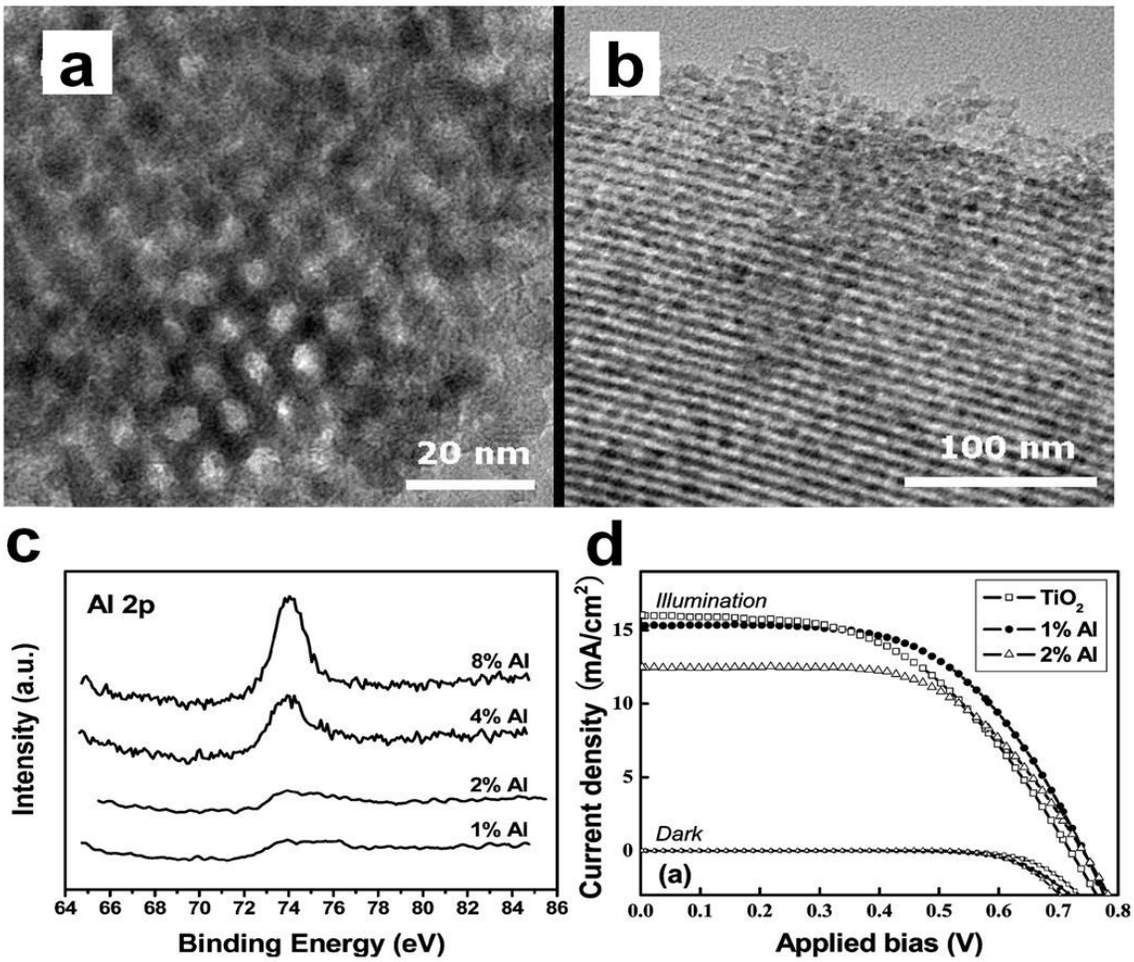


**Figure 4.** a-b) TEM images of mesoporous $TiO_2$, illustrating the ordered mesopores. c) XPS spectra of mesoporous $Al_2O_3$/$TiO_2$ with various levels of Al calcined at 525°C. d) *J*-V curves in the illuminated and dark states of pure mesoporous $TiO_2$, 1 and 2 mol% $Al_2O_3$/$TiO_2$ (light intensity: 100 mW/cm$^2$; AM 1.5 filter; illumination area: 0.25 cm$^2$). (Kim et al., 2010).

D. Chen et al. did a good job on this area, and synthesized uniform, crystalline, and mesoporous $TiO_2$ beads in size of ~800 nm through a combination of sol-gel and solvothermal processes, which exhibited the surface area of 108.0 m$^2$/g and tunable pore sizes (pore diameter: 14.0 ~ 22.6 nm) (Chen et al., 2009). Due to the submicrometer-sized particle diameter and the high specific surface area, the mesoporous $TiO_2$ beads enhanced the LHE without sacrificing the accessible surface for dye loading, thereby increasing the PCE compared to P25 nanoparticles. The photoanode based on these mesoporous $TiO_2$ beads exhibited an overall light conversion efficiency of 7.20% ($V_{oc}$ = 0.777 V, $J_{sc}$ = 12.79 mA/cm$^2$, *FF* = 0.72), significantly higher than that derived from standard Degussa P25 $TiO_2$ electrode with similar thickness (5.66%).

In a further study, the group selected Ru(II)-based dye C101 and C106 to match with the mesoporous $TiO_2$ beads, and realized an overall PCE of greater than 10% ($\eta$=10.7%) using a single screen-printed $TiO_2$ layer cell construction (without an additional scattering layer). Hence, a delicate modulation of the micron/submicron size/ shape of mesoporous materials, and a careful selection of the dye to match the dye's photon-absorption characteristics with

http://dx.doi.org/10.5772/51633

the light scattering properties of the mesoporous materials, are important to improve the LHE and PCE of DSC (Sauvage et al., 2010).

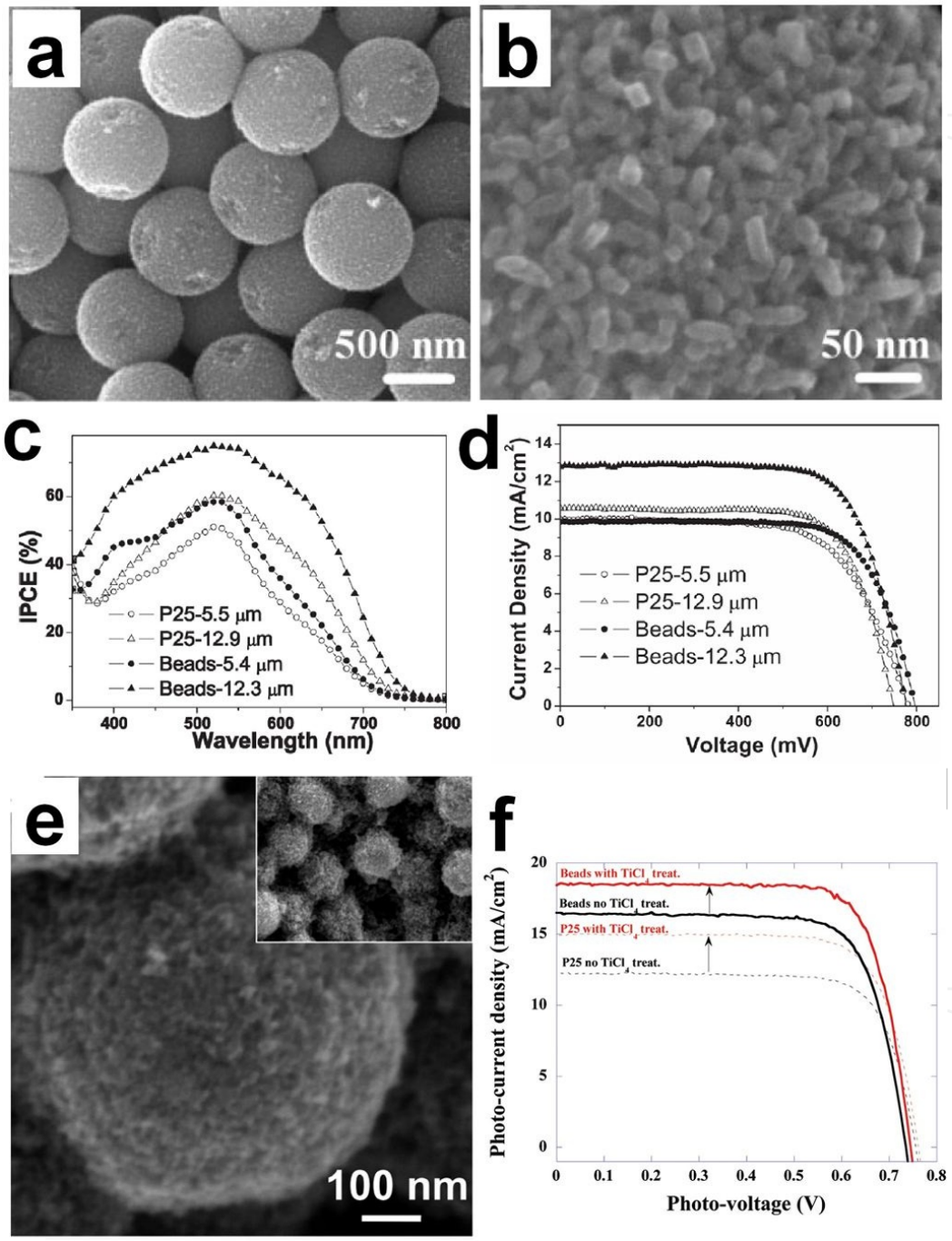


**Figure 5.** a-b) SEM images of the calcined mesoporous $TiO_2$ beads obtained after a solvothermal process with no ammonia for a) and 1.0 mL ammonia for b). c) IPCE curves and d) *J*-V curves of the $TiO_2$ electrodes prepared from P25 NPs and mesoporous $TiO_2$ beads with two film thicknesses. (Chen et al., 2009) e) SEM image of the screen-printed film composed of $TiO_2$ porous beads; f) *J*-V curves recorded at 100 mW/cm² of the 12 um thick film composed of P25 particles (dashed) or $TiO_2$ beads (solid) sensitized with the C101 dye without (in black color) and with $TiCl_4$ post-treatment (in red color). (Sauvage et al., 2010).

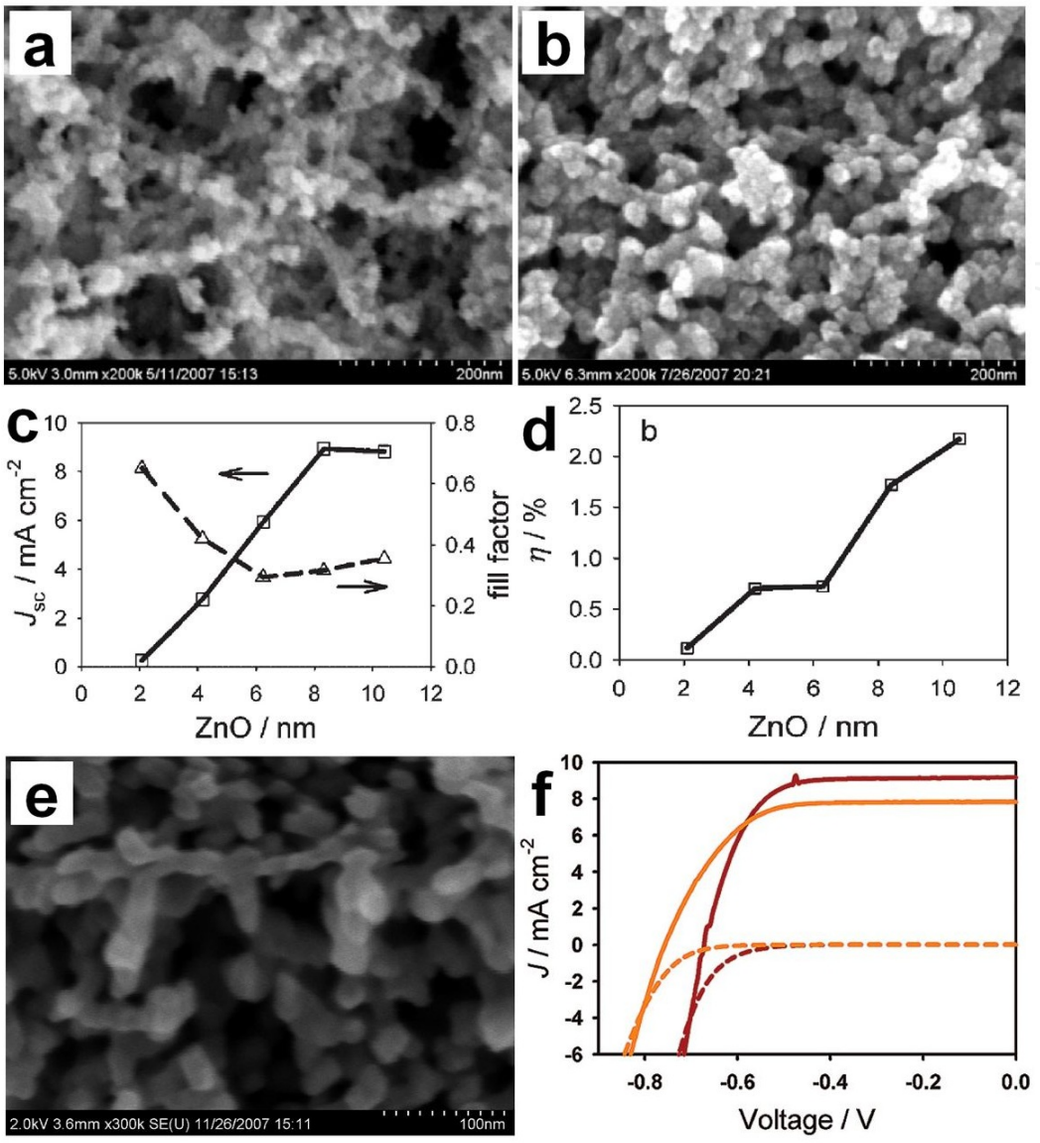


**Figure 6.** a-b) SEM images of aerogel frameworks coated with a) 4.4 and b) 8.4 nm ZnO. c-d) Plots of c) $J_{sc}$, *FF* and d) efficiency ($\eta$) as a function of thickness of ZnO deposited on aerogel frameworks. (Hamann et al., 2008a) e) SEM image of a ~30 µm thick aerogel film coated with 9.6 nm $TiO_2$. f) *J*-V curves for aerogel electrodes coated with 12 nm $TiO_2$ (Red) and $TiO_2$ nanoparticle (orange) in the dark (dasked lines) and under AM 1.5 illumination (solid). (Hamann et al., 2008b).

Among various mesoporous materials, aerogel is distinguished from others by its high surface area (100-1600 $m^2/g$) and light weight (0.003-0.5 $g/cm^3$) (Hüsing et al., 1998). The application of aerogel in the photoanode of DSC was pioneered by J. J. Pietron and J. T. Hamann in 2007-2008. The former work prepared the aerogel photoanode by the direct doctor-blading of the crushed $TiO_2$ aerogel particles, and demonstrated the IPCE of ~85% in the 500-600 nm range and ~52% at 700 nm for N719 sensitized photoanode (Pietron et al., 2007). Hamann et al. prepared $SiO_2$ aerogel film first via the supercritical drying process, and then coated ZnO or $TiO_2$ thin layer with controllable thickness via the atomic layer deposition (ALD) method (Hamann et al., 2008a, 2008b). They realized the aerogel based DSC devices with the efficiency of 2.4% (for ZnO cell) and 4.3% (for $TiO_2$ cell). Al-

http://dx.doi.org/10.5772/51633

so, the authors investigated systematically the effects of ZnO thickness on $SiO_2$ aerogel template on the photovoltaic performance, and found a nearly linear relationship between the key photovoltaic index and the thickness of ZnO layer (Figure 6c,d), with the optimal ZnO thickness of 10.5 nm. These results indicated that, on one hand, the aerogel film in combination of ALD or other physical or chemical deposition processes was a powerful candidate to prepare mesoporous photoanode with controllable microstructures. On the other, the use of the dangerous supercritical drying process in the synthesis of aerogel, together with the expensive and complicated ALD process involved in the preparation of $ZnO/TiO_2$ layer, limited the popularization of this method greatly. There were very few studies on the aerogel photoanodes in recent five years.

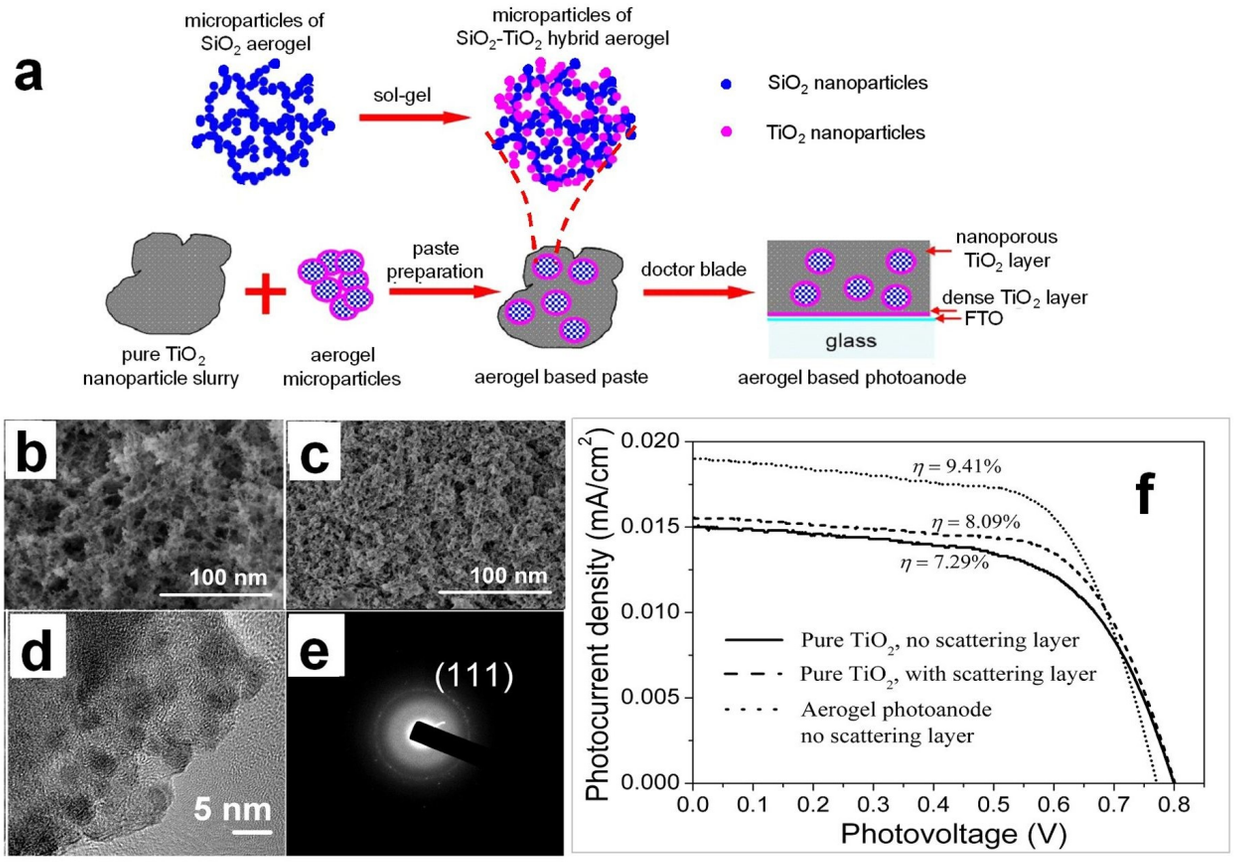


**Figure 7.** a) Schematic of the preparation of $SiO_2$-$TiO_2$ hybrid aerogel and aerogel based photoanode. SEM image of b) $SiO_2$ and c) $SiO_2$-$TiO_2$ hybrid aerogel (packing density: 0.037 and 0.125 g/cm$^3$). d) TEM image and e) SAED pattern of $SiO_2$-$TiO_2$ hybrid aerogel. f) *J*-*V* curves of DSC based on pure $TiO_2$ photoanode with and without scattering layer and aerogel modified photoanode. (Gao et al., 2012).

To crack above problems, X. D. Gao et al. developed a low-cost sol-gel and ambient-drying route to fabricate $SiO_2$-$TiO_2$ hybrid aerogels, which possessed a very high surface area of 500-1170 m$^2$/g, and incorporated them into nc-$TiO_2$ electrode, obtaining the aerogel hybrid photoanodes (Gao, et al., 2012). These hybrid photoanodes yielded significantly higher photocurrent densities than nc-$TiO_2$ photoanodes due to the increased dye-loading

capacity and the enhanced visible scattering effect, showing the highest efficiency of 9.41% at optimal condition, 16% higher than the $TiCl_4$-treated $TiO_2$ photoanode modified with a conventional scattering layer. This work indicated that, the hybrid photoanodes integrating both the high-surface-area mesoporous materials and nc-$TiO_2$ represented a powerful and viable route toward high-efficiency DSCs.

In brief, current studies on the mesoporous photoanodes built up by the high-surface-area mesoporous materials have unambiguously proved that, the application of high-surface-area powders/beads/aerogel in the photoanode can effectively increase the dye-loaing capacity and the light scattering of the electrode, and correspondingly improve the LHE of DSC in most cases. The preparation of mesoporous materials with regular and uniform size/shape in micron/submicron scale, and their integration with nc-$TiO_2$ or other nanostructures, seem feasible to achieve high conversion efficiency. A remaining problem in these high-surface-area mesoporous materials is the inferior electron-transporting property, intrinsically originating from their lower particle coordination number than the common nc-$TiO_2$ porous electrode. A possible solution may be the development of hybrid electrodes by incorporating metal, carbon nanotube, or graphene etc into the mesoporous structures. A mesoporous material possessing both high surface area and good conductivity is by all means necessary for highly efficient DSCs.

## 4. Hierarchical photoanodes

Hierarchical nanostructures, those with different morphology at different length scale and usurally characterized by the high surface area, are intresting candidates for efficienct photoanodes in DSC. This special class of nanostrcutures is spurred at the low surface area and consequently the low PCE of nanowire based photoandes, and have receivd wide-spread and intensive studies in recent years. Hierarchical ZnO and $TiO_2$ in the form of grass, forest, popborn ball, and tube etc. have been developed, and a wide range of chemical and physical methods have been used to prepare the hierarchical structures, including the hydrothermal synthesis, sol-gel, chemical bath deposition, pulsed laser deposition, photolithography, and so on. Due to the huge literature in this field, here we merely present some representive results in recent three years.

ZnO nanowire array may be the piorneer in the nanostructured photoanode since the outstanding work of M. Law et al. (Law et al., 2005). However, the PCE of nanowire based photoanode was low (mostly 1%-3% for a long time) mainly due to its low surface area. So the development of hierarchical ZnO and their application in DSC are wide-spread recently. As an example, Xu et al. reported a two-step synthesis process to produce hierarchical ZnO nanoarchitectures (Figure 8a,b), in which ZnO nanosheet arrays were first prepared by the pyrolysis of the precursor $Zn_5(OH)_8Cl_2$ electrodeposited on conductive glass substrates, and then dense ZnO nanowires were grown on the surfaces of the primary ZnO nanosheets by the chemical bath deposition method (Xu et al., 2010). Due to the better dye loading through the increased internal surface area and the higher light scattering behavior through extend-

http://dx.doi.org/10.5772/51633

ing the optical path length within the photoanode, the DSC based on the hierarchical ZnO nanowire-nanosheet architectures showed a PCE of 4.8%, nearly twice as high as that of DSC constructed using a photoanode of bare ZnO nanosheet array.

Apart from these hierarchical structures with relatively simple structures, several groups developed ZnO or $TiO_2$ forest (Figure 8c,d), more complicated hierarchical structures. F. Sauvage et al. prepared the hierarchical assemblies of nanocrystalline particles of anatase $TiO_2$ (Sauvage et al., 2010), by a pulsed laser deposition method, via the fine modulation of the plasma expansion dynamics by means of a reactive atmosphere during the ablation process. In combination with the high molar extinction coefficient heteroleptic C101 dye, the authors achieved 3.1% power conversion efficiency for 2 um thick films and 5.0% for films 7 um thick, demonstrating the great potential of the physical vapor deposition method in growing hierarchical nanostructured photoanodes with high conversion efficiency.

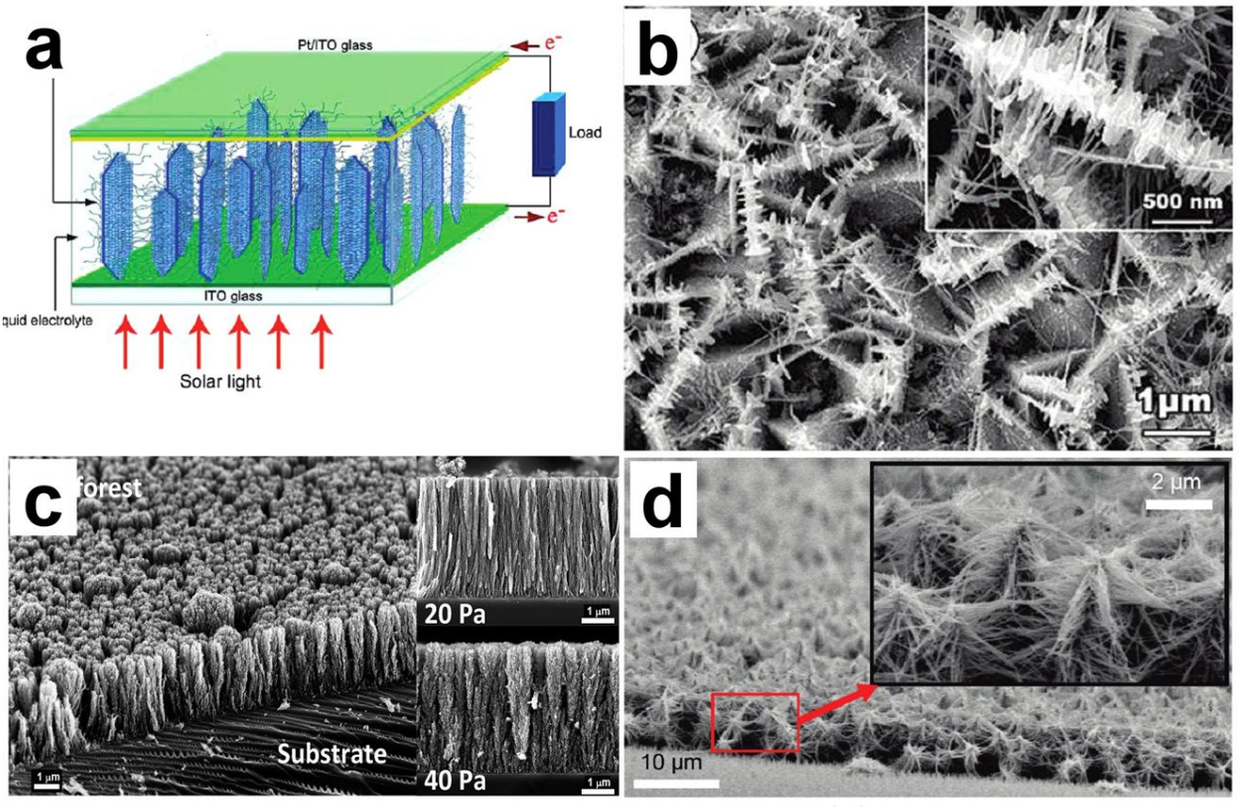


**Figure 8.** a) Schematic of ZnO hierarchical nanostructures derived from ZnO nanosheet arrays and b) top-view SEM image of ZnO nanowire-nanosheet architectures obtained by aqueous chemical growth after 4 h. The inset of b) corresponds to the magnified image. (Xu et al., 2010) c) $TiO_2$ forest-like films grown by pulsed laser deposition: (left) overview of a film deposited at 40 Pa; (right) cross sections of films deposited at 20 and 40 Pa. (Sauvage et al., 2010) d) SEM image of ZnO nanowire nanoforest (tilted view). (Ko et al., 2011).

Meanwhile, using the traditional hydrothermal method integrating with the simple selective hierarchical growth sequence, S. Ko et al. demonstrated ZnO nanoforest photoanode with high density, long branched treelike multigeneration hierarchical crystalline ZnO nanowires (Figure 8d) (Ko et al., 2011). The DSC exhibited almost 5 times higher than the efficiency of

DSCs constructed by upstanding ZnO nanowires (2.63% v.s. 0.45%). The enhanced surface area for higher dye loading and light harvesting, and the reduced charge recombination by providing direct conduction pathways along the crystalline ZnO "nanotree" multi generation branches, were responsible for the efficiency improvement.

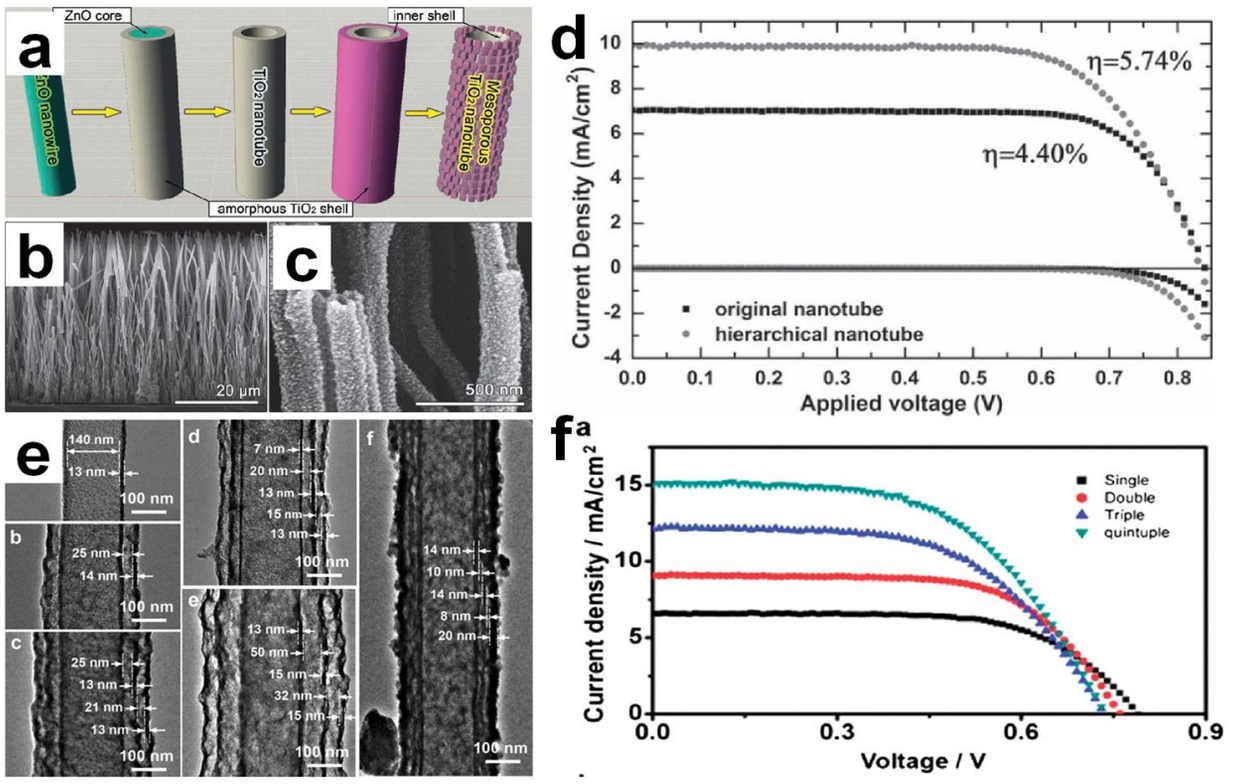


**Figure 9.** a) Schematic of the preparation of hierarchical $TiO_2$ NTA: beginning with a ZnO nanowire and followed by multiple procedures of $TiO_2$ coating, ZnO core removal, subsequent $TiO_2$ coating, and hierarchical derivation to a double-shell architecture. b) cross-section SEM image of $TiO_2$ nanotube array with 41 um thickness and c) magnified SEM image of hierarchical $TiO_2$ nanotube. d) *J–V* curves of the nanotube DSCs prepared with 20-μm thick nanotube arrays with the original and hierarchical structure. (Zhuge et al., 2011) e) TEM images of triple-shelled $TiO_2$ NTs with different structural features. f) *J*–V curves of DSCs based on multi-sheel $TiO_2$ nanotube electrodes. (Qiu et al., 2012).

Nanotube array (NTA) is another type of hierarchical structures receiving great attention, which is developed on the basis of nanowire in view of its much higher surface area than nanowire. Currently, the hierarchical $TiO_2$ NTA has becoming an intensive research branch. Different from the traditional synthesis of $TiO_2$ nanotube via the anodic oxidation, F. Zhuge et al. reported the synthesis of vertically aligned $TiO_2$ NTAs (up to 40 um) on FTO by using ZnO nanowire array as the hard template, and demonstrated the hierarchical derivation for effective surface area enhancement in DSCs (Figure 9 a-c) (Zhuge et a., 2011). The distinctive double-shell structure of the nanotube provided both the high surface area and the high electron-transport path, showing the overall conversion efficiency of 5.7%, 50% higher than the original nanotube (Figure 8d). In a further work, the group updated their multi-shell fabrication technology via ZnO nanowire template, and successfully obtained coaxial multi-shelled $TiO_2$ NTA with controllable shell numbers and shell thickness (Figure 9e) (Qiu et al.,

http://dx.doi.org/10.5772/51633

2012). Exhibiting the BET surface area of 119-331 $m^2/g$, DSC devices based on these multi-shelled NTA exhibited the highest efficiency of 6.2%, higher than that based on the single-layer $TiO_2$ nanotube array (3.35%) at similar experimental parameters (Figure 9f).

Apart from the hierarchical nanowire/nanotube array, there are also a few studies which modulate the pores in the photoanode to realize the hierarchical structures. C. Y. Cho et al. reported an interesting method to generate hierarchical electrodes consisting of meso- and macroscale pores (Cho et al., 2011). Mesoscale colloidal particles and lithographically patterned macropores were used as the dual templates, with the colloidal particles assembled within the macropores. An infiltration of $TiO_2$ into the template and subsequent removal of the template produced hierarchical $TiO_2$ electrodes for DSC (Figure 10a). While the holographic lithography defined the macroporous networks, the colloidal crystal templates provided three-dimensionally organized mesoscale pores with a uniform size distribution (Figure 10 b-e). Owing to the strong scattering and the suppression of charge recombination in the hierarchical $TiO_2$ electrodes, the photovoltaic performance of the cell was comparable with nc-$TiO_2$ electrodes, showing a maximum efficiency of 5.0% with 50 nm pores and 6 μm thickness.

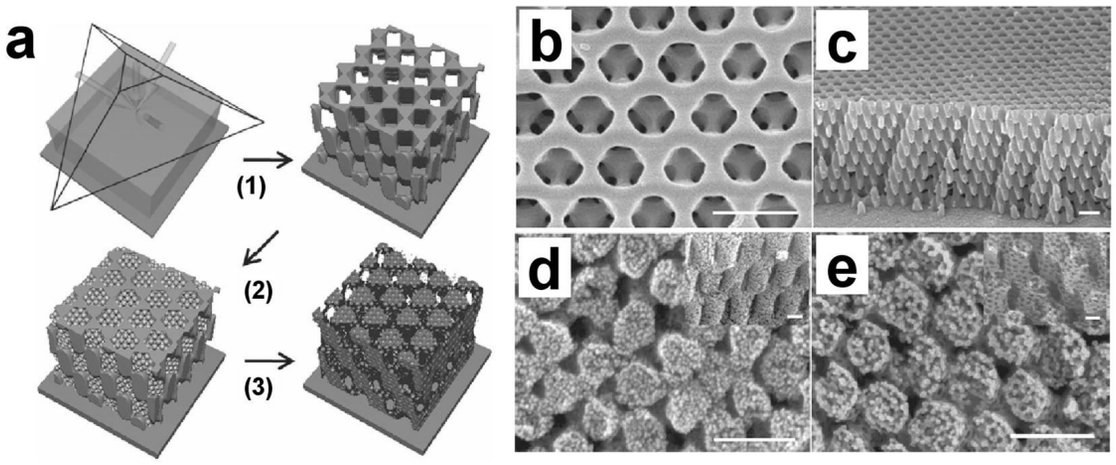


**Figure 10.** a) Schematic of the preparation of hierarchical $TiO_2$ electrode via double template method. (1) Formation of four-beam interference and the fabrication of the macroporous SU-8 structures. (2) Filling of the holographic patterns with mesoscale colloidal particles, and (3) Coating of precursors and removal of dual templates. SEM image of b) the surface and c) the cross-section of the macroporous SU-8 surface. SEM image of the hierarchical porous $TiO_2$ electrode from dual templates of SU-8 filled with colloidal particles with diameters of d) 60 nm and e) 110 nm. Scale bar: 1 μ m. (Cho et al., 2011).

In general, the hierarchical photoanodes, though possessing obviously higher internal surface area than the nanowire/nanotube/nanoplate counterparts and higher conductivity than nc-$TiO_2$ electrode, haven't show a predominant advantage over other materials up to now. The PCE of most photoanodes based on the hierarchical structures is still much lower than the state-of-the-art performance of nc-$TiO_2$ electrode. A possible vent for the hierarchical photoanodes may be the further increase of its internal surface area while maintaining its high electron-transporting nature. Also the combination of the hierarchical structures with the mesoporous material is a meaningful and feasible strategy.

## 5. Scattering layers on nc-$TiO_2$ electrode

The photoanode of DSC is traditionally composed of nc-$TiO_2$ film, which is basically transparent for visible light (Rayleigh scattering, mainly), resulting in a considerable part of light shone on the DSC transmitting through the $TiO_2$ layer without interacting with the sensitizer. To overcome this problem, scattering layers with different structures, including scattering centers and upper scattering layers, have been employed. The theoretical studies since 1998, and subsequent substantial experimental studies on scattering layers based on the submicron particles of $TiO_2$, $ZrO_2$, ZnO, nanowire, hierarchical structures, mesoporous spheres, photonic crystals, and upper-conversion materials, comprise a vivid picture about the research activities in this area. By briefing some important advances, we describe here some novel scattering layers developed in recent years.

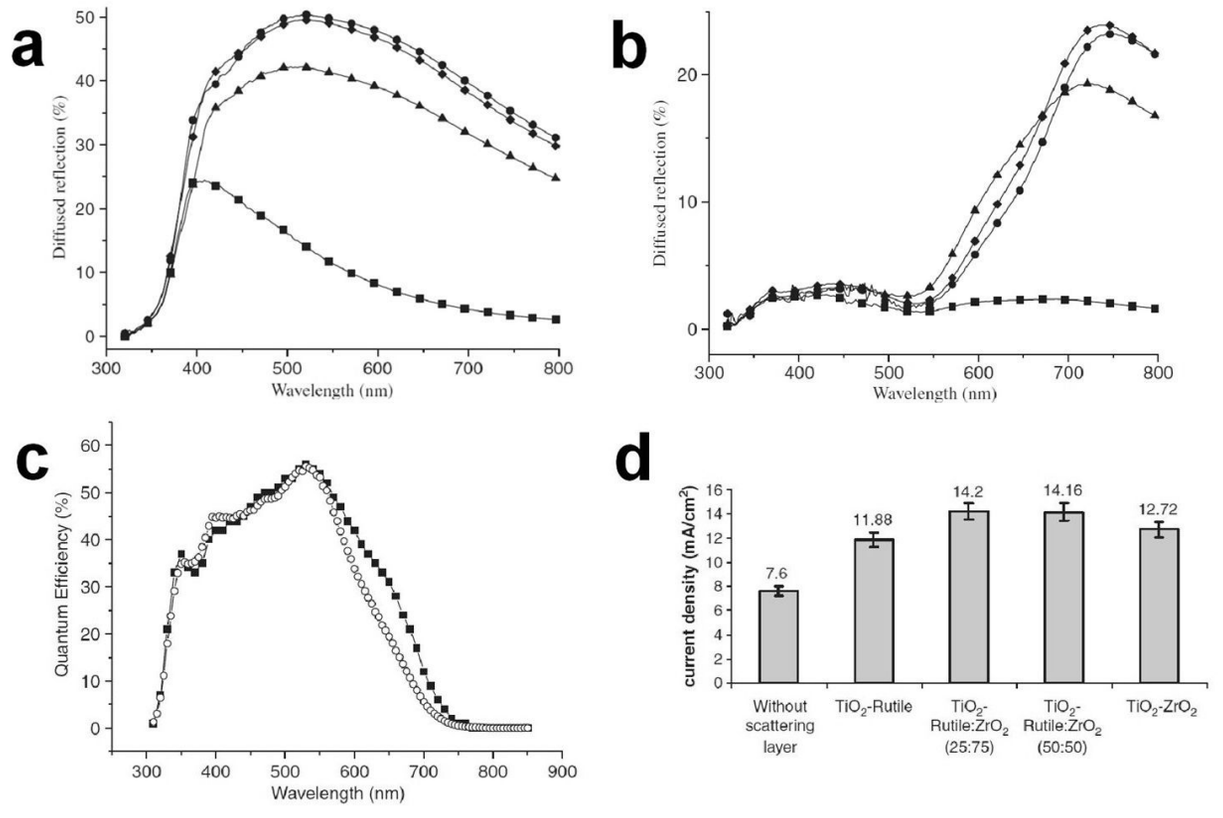


**Figure 11.** a-b) Diffused reflection spectra of a) undyed and b) sensitized $TiO_2$ layer without scattering layer (■), with the scattering layers of $TiO_2$-Rutile (▲), $ZrO_2$ (●) and 25:75 mixture of $TiO_2$-Rutile and $ZrO_2$ (◆). c) IPCE curves for devices with $TiO_2$ electrode with (■) and without (○) a scattering layer, the scattering layer being 25:75 mixture of $TiO_2$-Rutile and $ZrO_2$. d) Current densities obtained from devices with 4 mm thin layer of $TiO_2$ with and without scattering layers. The thickness of the scattering layers is ~6 um for all samples. (Hore et al., 2006).

In 1998, J. Ferber et al. started from Mie theory, and calculated the multiple scattering in $TiO_2$ electrodes using a numerical solution of the radiative transfer equation (Ferber et al., 1998). These calculations predicted that, a suitable mixture of small particles (20 nm), which

http://dx.doi.org/10.5772/51633

resulted in a large effective surface, and of large particles (250-300 nm), which were effective light scatterers, had the potential to enhance the solar absorption significantly.

In 2006, S. Hore et al. reported systematically the effects of $TiO_2/ZrO_2$ scattering layer on the photovoltaic performances (Hore et al., 2006). Different scattering layers composed of commercial $TiO_2$-Rutile (Bayer Germany) and $ZrO_2$ (TOSOH Corporation, Tokyo, Japan) with varied proportion were examined, providing an in-depth understanding on the functions of the top scattering layer. DSC device with an area of 2.5 $cm^2$ exhibited the PCE of 6.8% using an only 4 μm layer of $TiO_2$ electrode together with an optimal scattering layer, illustrating the potential of a suitable scattering layer on both the improvement of the efficiency and the reduction of the cost by using less sensitizer.

Very recently, F. E. Gaĺvez et al. reported an integral optical and electrical theoretical analysis on the effects of the different design of the diffuse light scattering on the performance of DSCs (Gaĺvez et al., 2012). Based on a Monte Carlo approach, they introduced the light harvesting efficiency and the electron generation function extracted from optical numerical calculations in a standard electron diffusion model, to obtain the steady-state characteristics of the different configurations considered (Figure 12). They proposed that the diffuse scattering layers acting as the back reflector provided the largest achievable light harvesting efficiencies, which determined an optimum overall performance, for electron diffusion lengths longer than the electrode thickness. When the electron diffusion length was shorter than the electrode thickness, the embedding of the diffuse scattering particles in the nanocrystalline paste yielded a better output even when the light harvesting was not optimal. These results can provide helpful guidance for us to design and prepare the scattering structure of the photoanode.

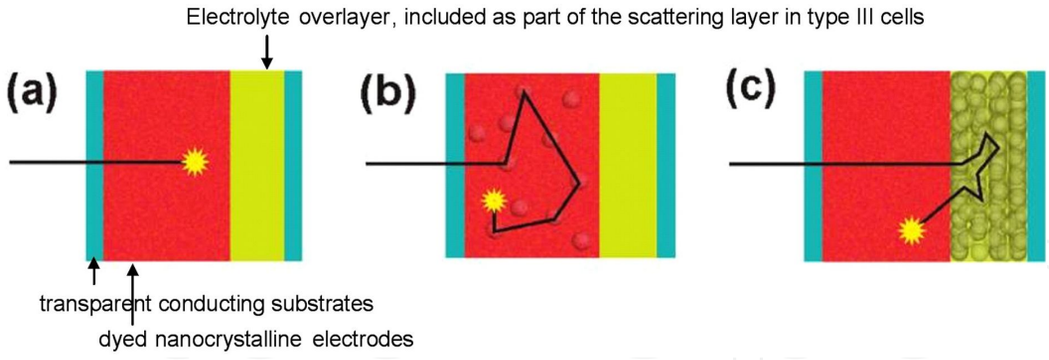


**Figure 12.** Simulated trajectories of a photon absorbed by a) standard semi-transparent cell, b) cell with an electrode embedding diffuse scattering particles, and c) cell made of a semi-transparent electrode coupled to a diffuse scattering layer, illustrating the different series of scattering events that yield longer optical paths and thus enhance the probability of absorption in each type of modified cell under consideration. (Gaĺvez et al., 2012).

In recent years, with the rapid development of nanostructured photoanodes, various nanostructures have been used as the top scattering layer of nc-$TiO_2$ electrode or the novel photoanodes based on nanowire/ nanotube arrays etc. For example, K Fan et al. applied $TiO_2$ fusiform nanorods (diameter: 20-80 nm, length: 200-400 nm) as the scattering layer of P25-based electrode (Figure 13), and observed 66.5% improvement in the efficiency with lower

resistance and longer electron lifetimes as compared to the bare P25-based solar cell (Fan et al., 2011). The reduced charge recombination and the sufficient scattering effect of the nanorods in the film electrode were responsible for this improvement.

Koo H. J. et al. prepared nano-embossed hollow spherical (NeHS) $TiO_2$ particles and investigated their photovoltaic property in DSC as the bifunctional scattering layer (Koo et al., 2008). The walls of the obtained hollow spheres were composed of nanocrystalline anatase $TiO_2$ particles with mesoporous structure (Figure 14 a-c), which endowed them 5 times higher dye-loading capacity (N719 dye: up to $5.0\times10^{-5}$ mol/g) than that of the normally used 400 nm-diameter scattering particles with flat surfaces. The NeHS particles scattered incoming light effectively as confirmed by the reflectance spectroscopy (Figure 14 d,e). When the NeHS $TiO_2$ particles were used as the secondary scattering layer in DSC, a substantial improvement in the efficiency has been achieved, with the highest conversion efficiency of 10.34%. Huang F et al. used the submicrometer-sized mesoporous $TiO_2$ beads as the dual function scattering layer for the nanocrystalline electrode, and observed similar results, demonstrating that the dual-function scattering layer represented a powerful alternative for the traditional large-particle scattering layer for high-efficiency DSCs (Huang et al., 2010).

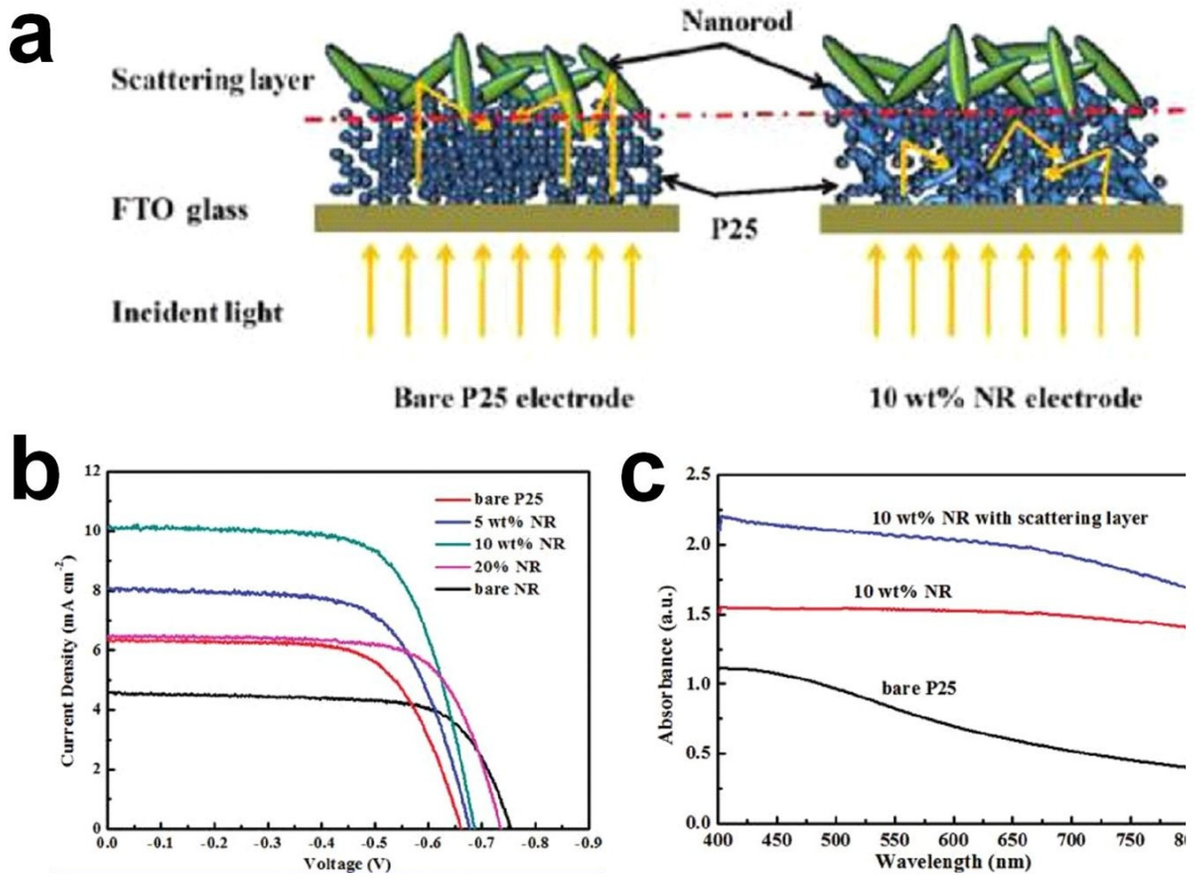


**Figure 13.** a) Schematic of the photoanodes with nanorod scattering layer. b) *J*-V curves of DSCs, and c) UV-VIS spectra of bare P25 film, and with different nanorod scattering layer. (Fan et al., 2011).

http://dx.doi.org/10.5772/51633

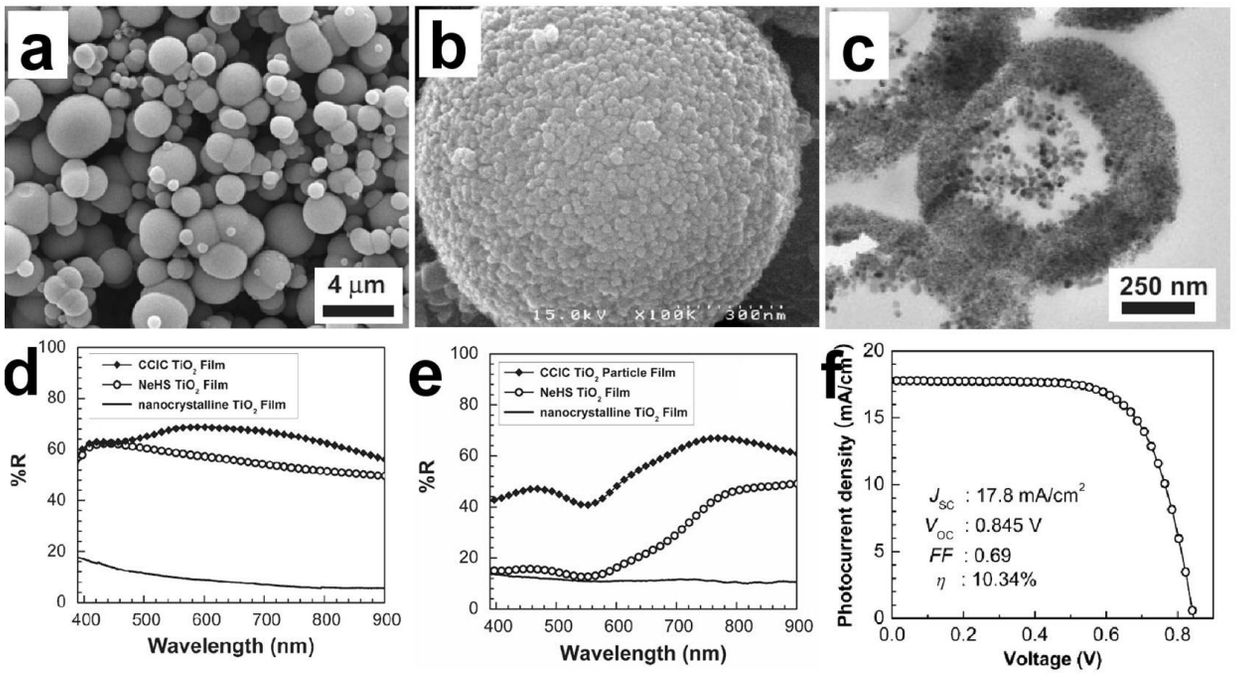


**Figure 14.** SEM image of a) the as-synthesized nano-emboded hollow sphere (NeHS) $TiO_2$ particles, b) high-magnification image for NeHS $TiO_2$ calcined at 450 °C. c) TEM image of a sliced NeHS $TiO_2$ particle. d-e) Diffused reflectance spectra of the nanocrystalline, CCIC, and NeHS $TiO_2$ particulate films d) without and e) with adsorbed N-719 dye. f) *J*-*V* curve of a DSC based on NeSH $TiO_2$ particulate film as an overlayer on a nanocrystalline $TiO_2$ film under AM 1.5G-one sun light intensity. (Koo et al., 2008).

Below we gave two examples which used the nanostructured scattering layer on the electrodes based on nanowire array or nanofibers. Shao et al. demonstrated an interesting double layer photoanode, with the bottom layer of $TiO_2$ nanorod array providing direct conduction pathway for photo-generated electrons, and the upper layer of micro-flowers built up by $TiO_2$ nanobelt, increasing the light harvesting ability as the scattering part (Shao et al., 2011). The cell based on this hierarchical anatase $TiO_2$ exhibited a conversion efficiency of 5.53%, superior than commercial $TiO_2$ (P25). The much higher optical reflectance of the hierarchical structures than the nanorod array and nanoparticle films (Figure 15) proved that this morphology was beneficial to the light-scattering capacity of the photoanode.

Yang et al. reported an innovative bilayer $TiO_2$ nanofiber photoanode, which combined both smaller (60 nm) and larger (100 nm) diameter $TiO_2$ nanofibers fabricated by electrospinning (Yang et al., 2011). The smaller diameter nanofiber (SNF) layer with a high surface-to-volume ratio was used to adsorb sufficiently dye molecules and directly transport electrons released from excited dyes. The bigger-diameter nanofi ber (BNF) layer worked as light scattering, adsorbed sufficient dye molecules for energy harvest, and provided higher pore volume in BNF to facilitate electrolyte diffusion for regenerating sensitized dye molecules in the photoanode. Therefore, this bilayer composite nanostructure photoanode offered excellent dye-loading, lightharvesting, and electron-transport properties. The PCE of DSC was improved from 7.14% for the single-layer to 8.40% for the bilayer of $TiO_2$ nanofiber photoanode, representing an increase of 17%.

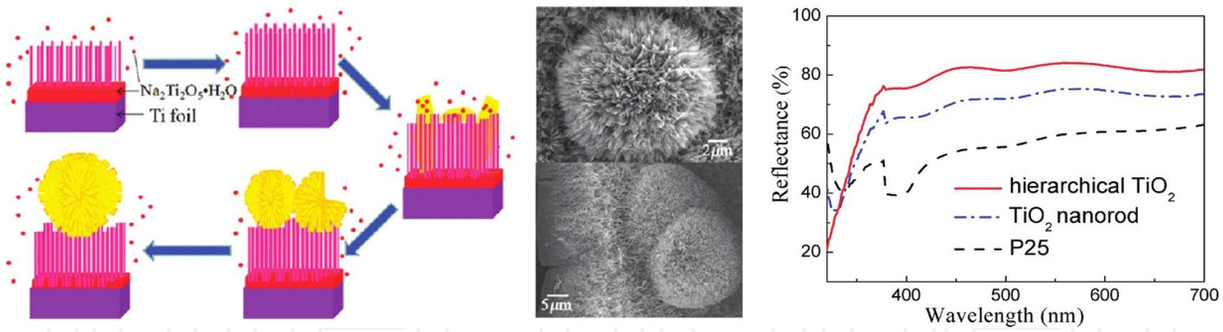


**Figure 15.** Schematic of $TiO_2$ nanorod array-micro flower hierarchical photoanode, SEM images of the photoanode at surface and cross section, and reflectance spectra of three kinds of $TiO_2$ photoanode on FTO substrate. (Shao et al., 2011).

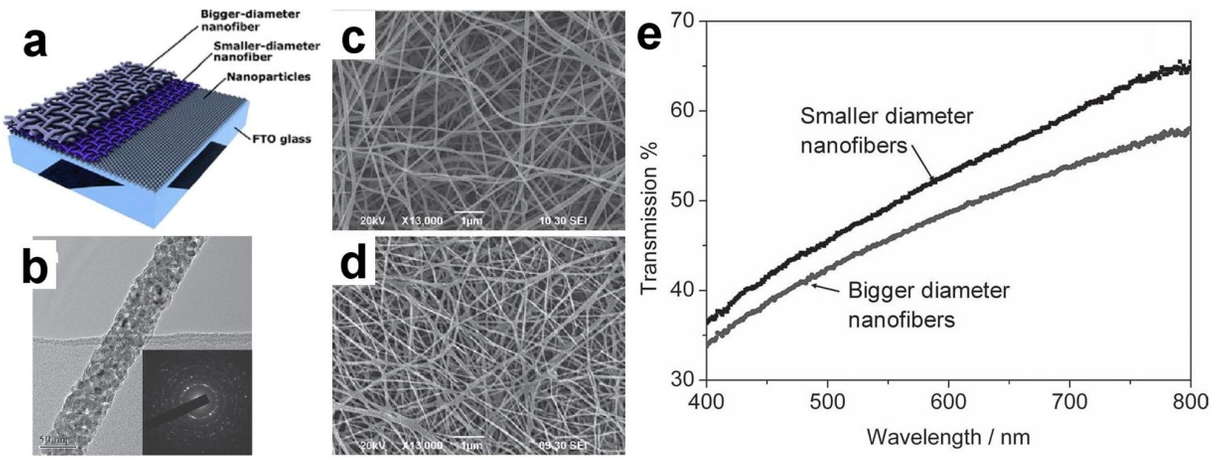


**Figure 16.** a) Schematic of the photoanode based on bi-layer electronspinned $TiO_2$ nanofibers. b) TEM image of smaller nanofiber and corresponding SAED pattern. c-d) SEM images of c) smaller and d) bigger nanofibers. e) UV-VIS transmission spectra of smaller diameter and bigger-diameter nanofiber photoanode with the same thickness (Yang et al., 2011).

As the conclusion of this section, we introduce a special scattering layer using up-converting materials. G. B. Shan et al. utilized the hexagonal nanoplatelets of β-$NaYF_4$:$Er^{3+}$/$Yb^{3+}$, a typical up-conversion phosphor owing to $Er^{3+}$ doping with $Yb^{3+}$ codopant assisting in the energy transfer process, as the second layer on nc-$TiO_2$ electrode (Figure 17) (Shan et al., 2011). Approximately 10% enhancements of photocurrent and overall DSC efficiency were achieved by the addition of the external layer, which exhibits two functions of light reflecting and near-infrared (NIR) light harvesting. Though the overall PCE of the cell and the improvement were moderate, the work opened a new opportunity to use some advanced functional materials to enhance the light-harvesting functions of DSC.

In summary, a wide variety of nanostructures including submicron particles, nanowires, nanofibers, mesoporous beads, spheres, nanopalletes etc have been used as the top scattering layer of DSC, which are proved to be very effective in improving the LHE and PCE of DSC, especially for the dual-function materials possessing both high surface area and large-

http://dx.doi.org/10.5772/51633

particle size. At the same time, the application of multiple function materials such as the up-converting nanopalletes in the scattering layer sheds a new light for further development.

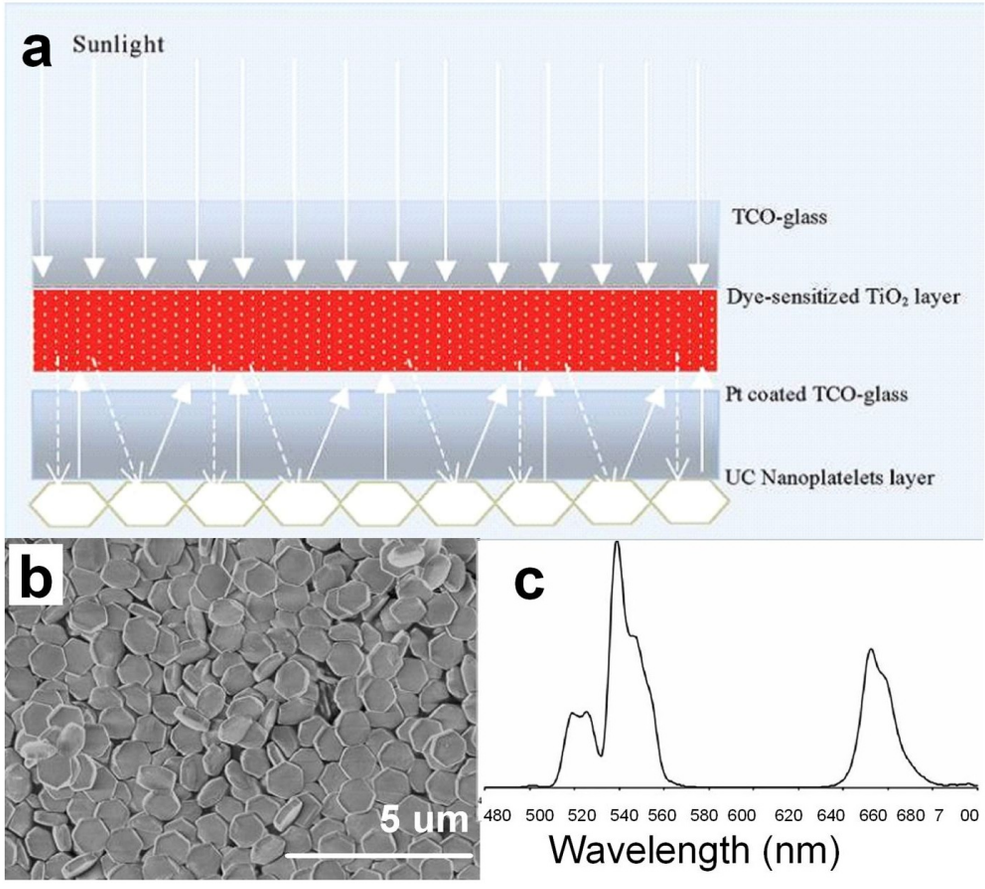


**Figure 17.** a) Schematic of the DSC device consisting of one internal $TiO_2$ transparent layer plus an external rear layer of β-$NaYF_4$:$Er^{3+}$/$Yb^{3+}$ nanoplatelets. b) SEM image and c) up-conversion fluorescence spectrum of the β-$NaYF_4$:$Er^{3+}$/$Yb^{3+}$ nanoplatelets. (Shan et al., 2011).

## 6. Plasmonic DSCs

Localized surface plasmon resonance (LSPR) behavior is an intriguing characteristic of metal nanoparticles (NPs), which is generated by the resonance between electric fields of electromagnetic waves and free electrons in metal NPs. The use of plasmonic effects has been proposed as a promising pathway to increase the light absorption in active layers of solar cells, and has been demonstrated on several thin-film solar-cell materials such as amorphous silicon, gallium arsenide, polymers, and DSC. Previous studies on the plasmonic solar cells with thin active layers have proved the beneficial functions of the LSPR on the photocurrent density through such following channels:

1. excitation of localized surface plasmon resonances of metallic NPs;

2. scattering of light by metallic NPs into dielectric-like waveguide modes of the solar cell;
3. coupling to propagating surface plasmon polariton (SPP) modes (Ding et al., 2011).

This has established a solid foundation for the rapid development of plasmonic DSCs in recent years.

The mostly-used metal NPs in the plasmonic DSCs are Ag and Au. While earlier studies have found the corrosion of metal particle in the electrolyte or the undesired introduction of electron-hole recombination by the plasmonic particles, it has become a common practice to protect the Ag or Au NPs by a thin $TiO_2$ or $SiO_2$ layer. Coupled with the standard thick nc-$TiO_2$ electrode, these plasmonic photoanodes performed fairly well compared with the control samples.

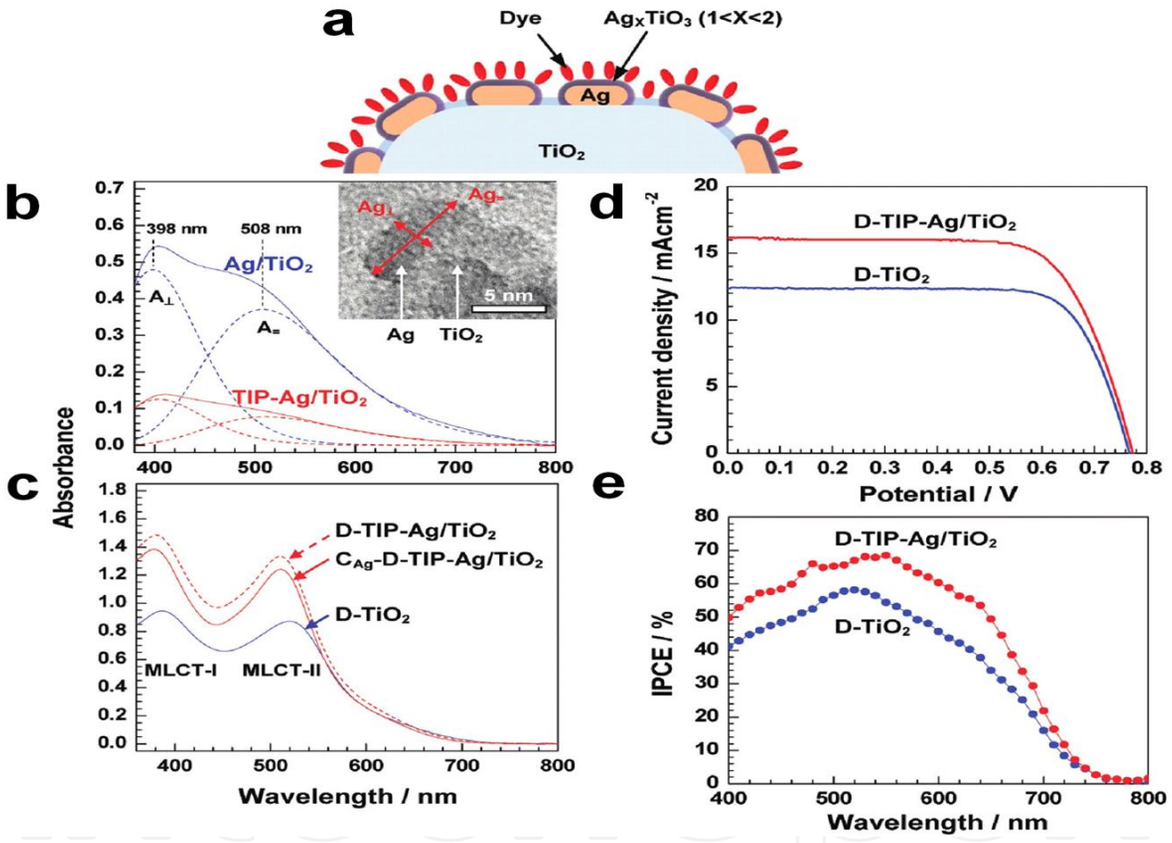


**Figure 18.** a) Schematic of Ag NPs deposited on $TiO_2$ NPs. b) Plasmonic absorption spectra of Ag NPs in Ag/$TiO_2$ (blue solid curve) and TIP-Ag/$TiO_2$ (red solid curve). Each spectrum is decomposed into two absorption peaks depending upon the geometry of Ag NPs. The inset shows a TEM image of the side view of Ag NP on $TiO_2$. $Ag_\perp$ and $Ag_=$ indicate the direction in the geometry of Ag NP. c) UV-VIS absorption spectra of D-$TiO_2$, D-TIP-Ag/$TiO_2$, and $C_{Ag}$-D-TIP-Ag/$TiO_2$. d) *J*-V and e) IPCE curves of D-$TiO_2$ and D-TIP-Ag/$TiO_2$ photoanodes. TIP-Ag: $TiO_2$ coated Ag NPs; D-$TiO_2$: N719 dye sensitized $TiO_2$ electrode; $C_{Ag}$-D-TIP-Ag/$TiO_2$: the extinction spectrum after removing the contributions of Ag NPs from the spectrum of D-TIP-Ag/$TiO_2$. (Jeong et al., 2011).

N. C. Jeong et al. provided a detail examination on the effects of the protection of Ag NPs on the LSPR and the cell performance (Jeong et al., 2011). They deposited Ag NPs on $TiO_2$ framework via the photo-reduction of $Ag^+$ from dissolved $AgNO_3$, and protected them by

http://dx.doi.org/10.5772/51633

a thin $TiO_2$ layer by refluxing Ag-$TiO_2$ electrode in isopropyl alcohol and subsequent annealing at 370°C. The electrode incorporating the protected silver NPs (Ag-$TiO_2$) showed enhanced extinction of a subsequently adsorbed dye (the ruthenium-containing molecule, N719), realizing an overall conversion efficiency of 8.9% and 25% improvement over the performance of otherwise identical solar cells incorporating silver NPs lacking protection (Figure 18). Roughly half the improvement could be traced to the increased dye loading by the photoanodes following silver incorporation, with the remaining improvement coming from the localized surface plasmon resonance (LSPR) enhancement of the effective absorption of N719 dye molecules.

J. Qi et al. coated $TiO_2$ thin layer (~2 nm) on Ag NPs and incorporated this Ag@$TiO_2$ nanostructures into the $TiO_2$ photoanode (Qi et al, 2011), which can easily transferred the carriers to surrounding $TiO_2$ NPs in contact with the shell, while providing a good protection for the metal NPs. By utilizing Ag@$TiO_2$ core-shell nanostructures, the optical absorption of dye molecules in solution and in thin film was enhanced by the strong localized electric field generated by LSPs (Figire 19 a,b). By incorporating Ag@$TiO_2$ NPs, the PCE of DSCs with very thin photoanodes (1.5 μm) was increased from 3.1%to 4.4%, and a small amount of Ag@$TiO_2$ NPs (0.1 wt%) improved efficiency from 7.8% to 9.0% while decreasing the photoanode thickness by 25% for improved electron collection (Figure 19c,d).

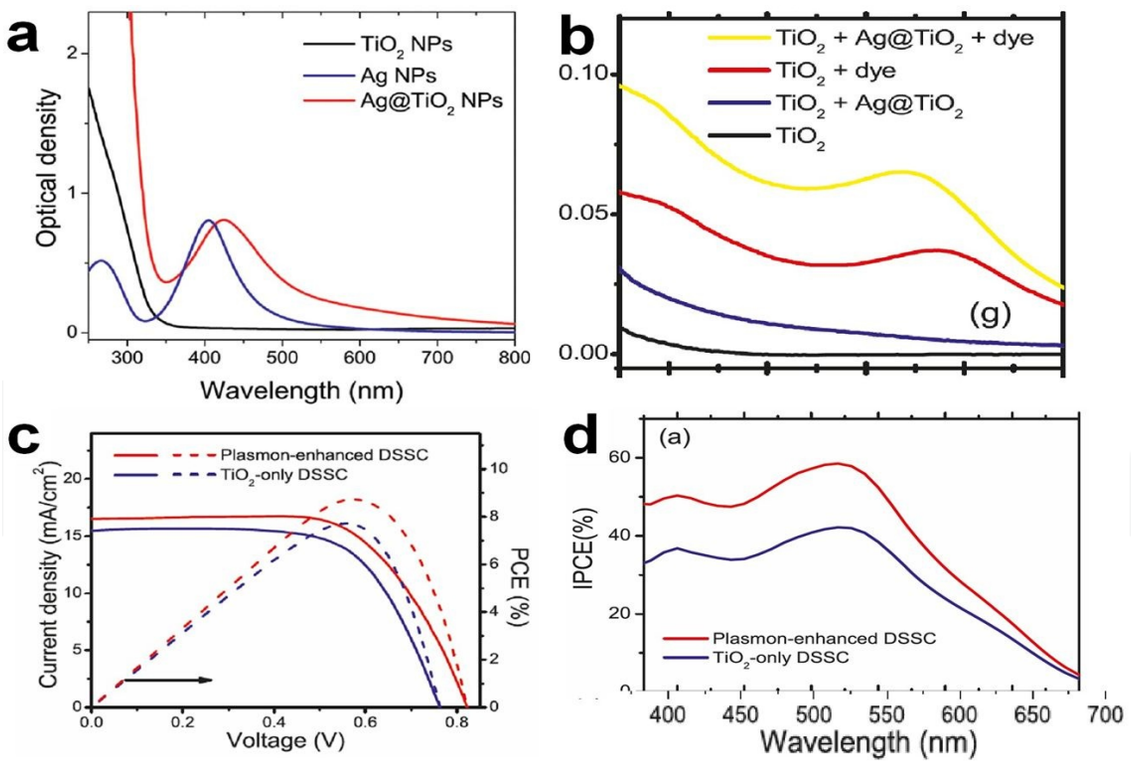


**Figure 19.** a) Absorption spectra of Ag NPs solutions stabilized by PVP, $TiO_2$ NPs, and Ag@$TiO_2$ NPs. b) Absorption spectra of Ag@$TiO_2$ NPs, dye, and their mixtures in $TiO_2$ film. c) *J*-V curves of plasmonic DSC (Ag/$TiO_2$ = 0.1 wt %, $\eta$ = 9.0%, *FF* = 67%, 15 μm) and $TiO_2$-only DSC ($\eta$ = 7.8%, *FF* = 66%, 20 μm). d) IPCE spectra of the DSCs with and without Ag@$TiO_2$. (Qi et al, 2011).

M. D. Brown et al. integrated Au NPs, which exhibited intense absorption due to the surface plasmon resonance in the visible band, into both the liquid and solid state DSCs (Brown et al., 2011). They successfully overcame the detrimental effects of the incorporating "bare" metal NPs into the bulk DSCs, by coating the Au NPs with a thin shell of silica, which could sustain the sintering process of the $TiO_2$ with negligible influence to the optical properties, resist the corrosion from the iodide/triiodie electrolyte, and enhance the photocurrent generation and solar cell performance as a result of light harvesting by the metal NPs. With a significant increase in the shortcircuit photocurren, the best solid state plasmonic cell sensitized with Z709 exhibited a PCE of 4.0% (Figure 20). The readily tunable optical properties of metallic NPs, through the use of structures such as nanobars, nanostars, or other complex shapes, provided extensive scope for further work to fully optimize the technology.

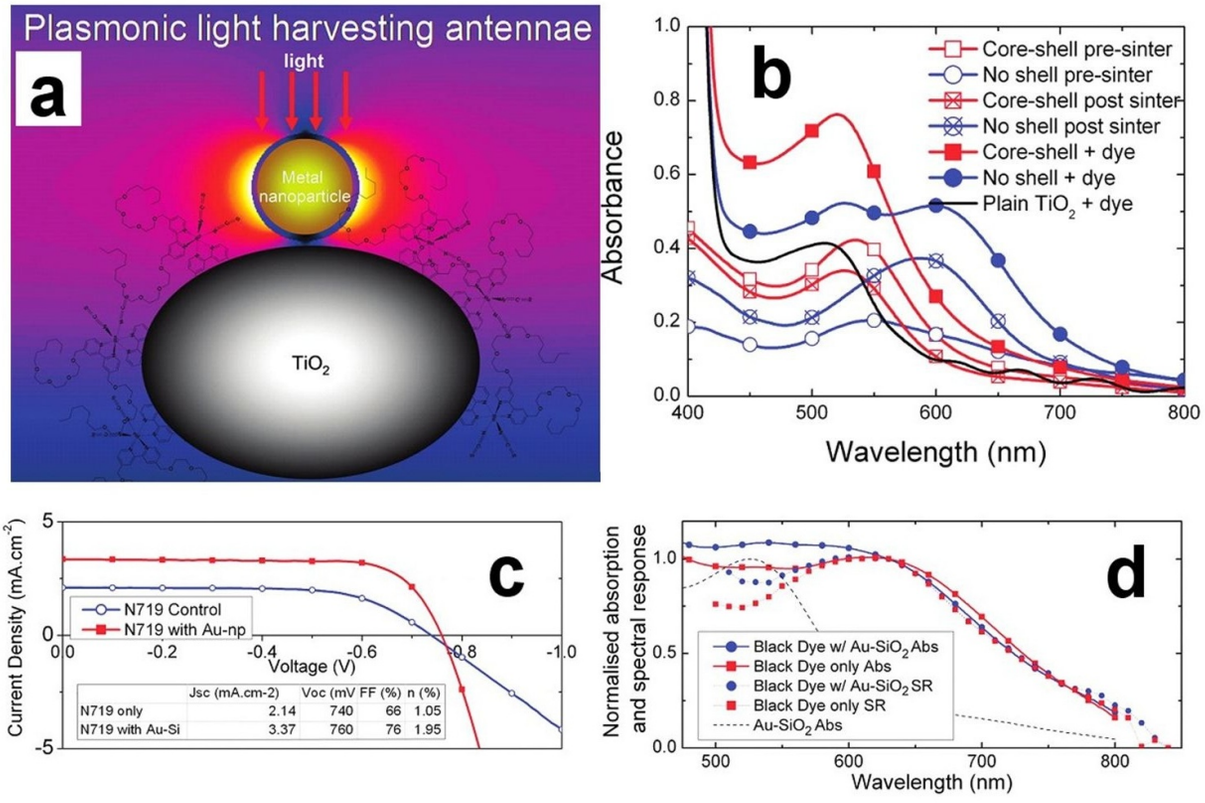


**Figure 20.** a) Schematic of plasmonic Au-$TiO_2$ structures. b) Absorption spectra of thin films (~1 μm) processed with nc-$TiO_2$ paste at different fabrication stages, including directly after doctor blade coating (pre-sinter), after two sintering cycles at 500°C and a $TiCl_4$ treatment (post-sinter), with final sensitization of Z907 (dye), $TiO_2$ paste incorporating bare Au NPs, Au-$SiO_2$ core shell NPs, and nc-$TiO_2$ film sensitized with Z907. c) *J*-*V* curves of liquid DSC (N719 sensitization, 1.1 μm thickness), with and without Au-$SiO_2$ core (15 nm)-shell (3 nm) nanoparticles. d) Normalized absorption (as 1-transmission-reflection) and spectral response of liquid DSCs. (Brown et al., 2011).

H. Choi et al. investigated the effects of the oxide capping layer of Au nanoparticles on the performance of plasmonic DSCs (Choi et al., 2012). By employing $SiO_2$- and $TiO_2$-capped Au NPs, they improved the cell efficiency from 9.3% for an N719 sensitized device to 10.2% upon incorporation of 0.7% Au@$SiO_2$ and to 9.8% upon loading of 0.7% Au@$TiO_2$ NPs. The

http://dx.doi.org/10.5772/51633

plasmonic effect was observed in $Au@SiO_2$ incorporated DSC, which produced higher photocurrent (Figure 21). However, in $Au@TiO_2$ incorporated DSC, Au NPs underwent charge equilibration with $TiO_2$ NPs and shifted the apparent Fermi level of the composite to more negative potentials, which resulted in a higher photovoltage. These observations opened up new opportunities to introduce both these paradigms and to synergetically enhance the photocurrent and photovoltage of DSC.

In brief, the plasmonic photoanodes are still a newly-emerged research area in DSC, spanning a wide range of materials (metal, semiconductor) and optical and electrochemical phenomena (localized surface plasmon resonance, scattering, electron-hole recombination). It is currently the main task for scientists to seek a suitable plasmonic structures (metal-oxide core-shell structures) and effective strategies to incorporate them into the nanocrystalline or nanostructured electrodes. While at present the nanoparticles of Au and Ag have been attempted to produce plasmonic DSC, further efforts may be extended to other metals (Ti, Zn, etc.) or morphologies with complex structures of metals (cubic, hexagonal, star-form etc.). Also, in-depth explorations on the mechanism of the plasmonic resonance embedded in the nanoporous electrode, and their detail influences on the photo-to-electric conversion process, are very useful to promote the development of this intriguing area.

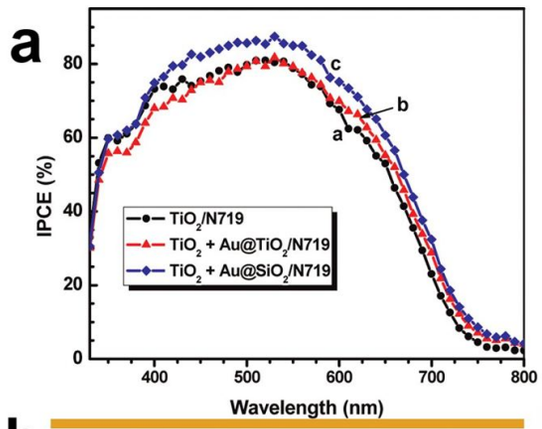


**b** **TABLE 1. Dye-Sensitized Solar Cell Performance**[a]

| support/dye | $J_{sc}$ (mA cm$^{-2}$) | $V_{oc}$ (V) | ff | $\eta$ (%) |
|---|---|---|---|---|
| $TiO_2$/N719 | 18.28 | 0.729 | 0.697 | 9.29 |
| $TiO_2$+Au@$TiO_2$/N719 | 18.281 | 0.771 | 0.694 | 9.78 |
| $TiO_2$+Au@$SiO_2$/N719 | 20.31 | 0.727 | 0.691 | 10.21 |

[a] Performances of DSSCs were measured with 0.18 cm$^2$ working area under AM 1.5 illumination. Electrolyte: 0.6 M DMPIml, 0.05 M $I_2$, 0.1 M LiI, and 0.5 M *tert*-butylpyridine in acetonitrile. Au@$TiO_2$ and Au@$SiO_2$ loadings were kept at 0.7% by weight. ff and $\eta$ correspond to fill factor and power conversion efficiency, respectively. DMPIml, 0.05 M $I_2$, 0.1 M LiI, and 0.5 M *tert*-butylpyridine in acetonitrile. Excitation: AM 1.5 white light.

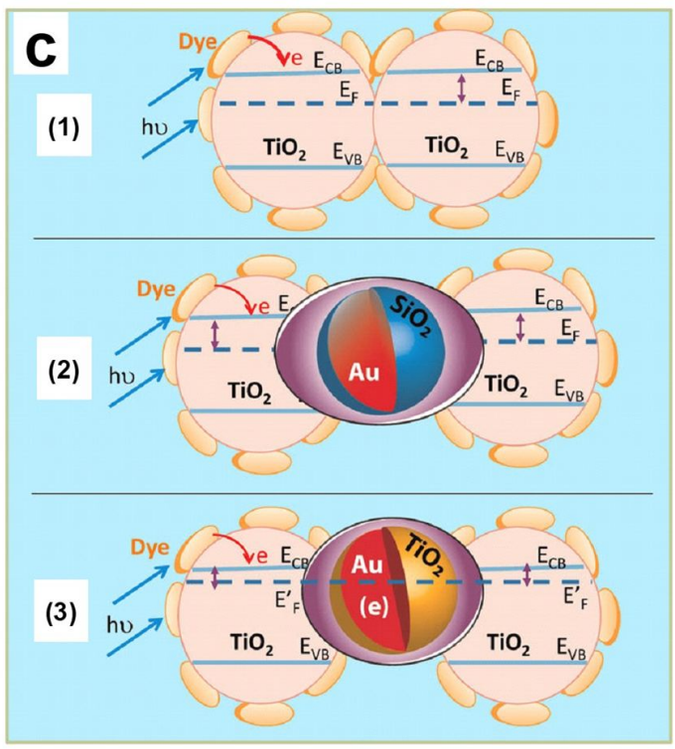


**Figure 21.** a) IPCE spectra of DSC employing N719 adsorbed onto $TiO_2$, $TiO_2$/Au@$TiO_2$, and $TiO_2$/Au@$SiO_2$ as photoanodes. The loading of core-shell particles is maintained at 0.7%. b) Photovoltaic performance of DSCs. c) Electron equilibration and its influence on the apparent Fermi level (EF): (1) dye $TiO_2$, (2) dye $TiO_2$/Au@-$SiO_2$, and (3) dye $TiO_2$/Au@$TiO_2$. LSP influence is seen in both (2) and (3), and shift in Fermi level as a result of electron accumulation in the metal core is seen in only (3). (Choi et al., 2012).

## 7. Photonic crystals based photoanodes and more

Photonic crystals (PCs) are materials that exhibit periodicities in their refractive index on the order of the wavelength of light, and thus provide many interesting possibilities for "photon management" (John, 1987). PC layers can be coupled to the charge-generating layer of DSC, and increase the LHE via such following mechanisms,

1. photon localization and enhanced red light absorption near the edges of the photonic bandgap,
2. light reflection within the photonic bandgap at various angles, and
3. formation of photon resonance modes within the dye-sensitized layer (Yip et al., 2010).

Compared with the traditional scattering techniques using geometrical optic-based elements (incoherent scattering layers, or high-reflectivity metallic mirrors), the application of PCs can obtain a more significant improvement on the LHE via the delicate control of the reflected, diffracted, or refracted light passing through the cell, apart from the apparent advantage in obtaining the transparent and colorful DSC rather than the opaque ones. The major limitation for the incorporation of PCs (especially the self-assembled 3D PCs) into DSC is the incompatibility between the fabrication routes for the photonic structures and the photoanode. So in the current stage, the preparation technology of PCs and their coupling to nc-$TiO_2$ layer represent the emphasis of many studies. In this section, we give several examples of PC layer in DSC with distinctive features in their structure.

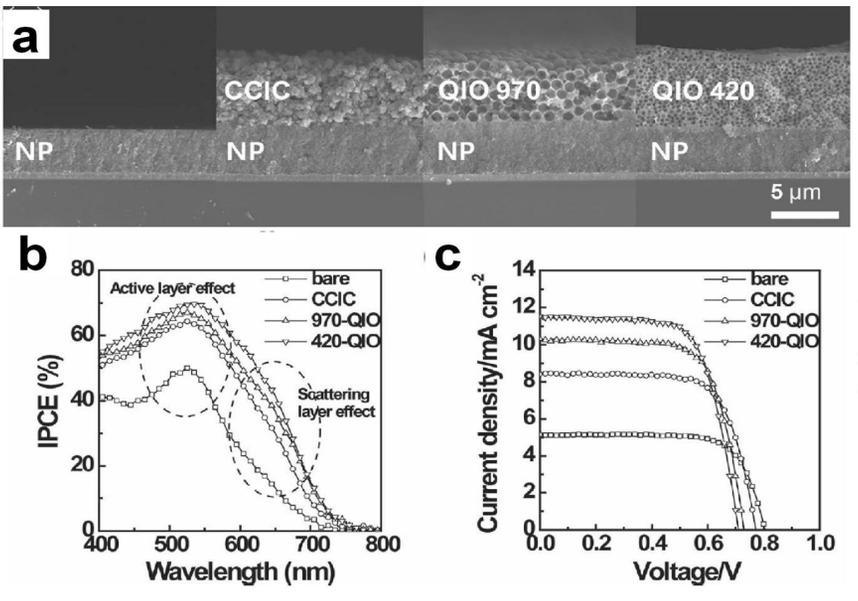


**Figure 22.** a) Cross-sectional SEM images of the photoelectrodes of nc-$TiO_2$ and with different scattering layers. b) IPCE spectra and c) *J–V* curves of the DSCs employing different scattering layers. (Han et al., 2011).

S. Han et al. fabricated quasi-inverse opal (QIO) layers with imperfect periodicity of hollows and applied them as the new scattering layer in DSC (Han et al., 2011). The porous QIO lay-

http://dx.doi.org/10.5772/51633

ers composed of highly crystalline anatase $TiO_2$ nanocrystals exhibited good dye-adsorptive properties and effective light-scattering properties over the wavelength range of 600–750 nm. The photocurrent of DSC based on the 420 nm-QIO layer was higher than the commercial scattering layer-based DSSC, achieving an efficiency of 5.7% (Figure 22).

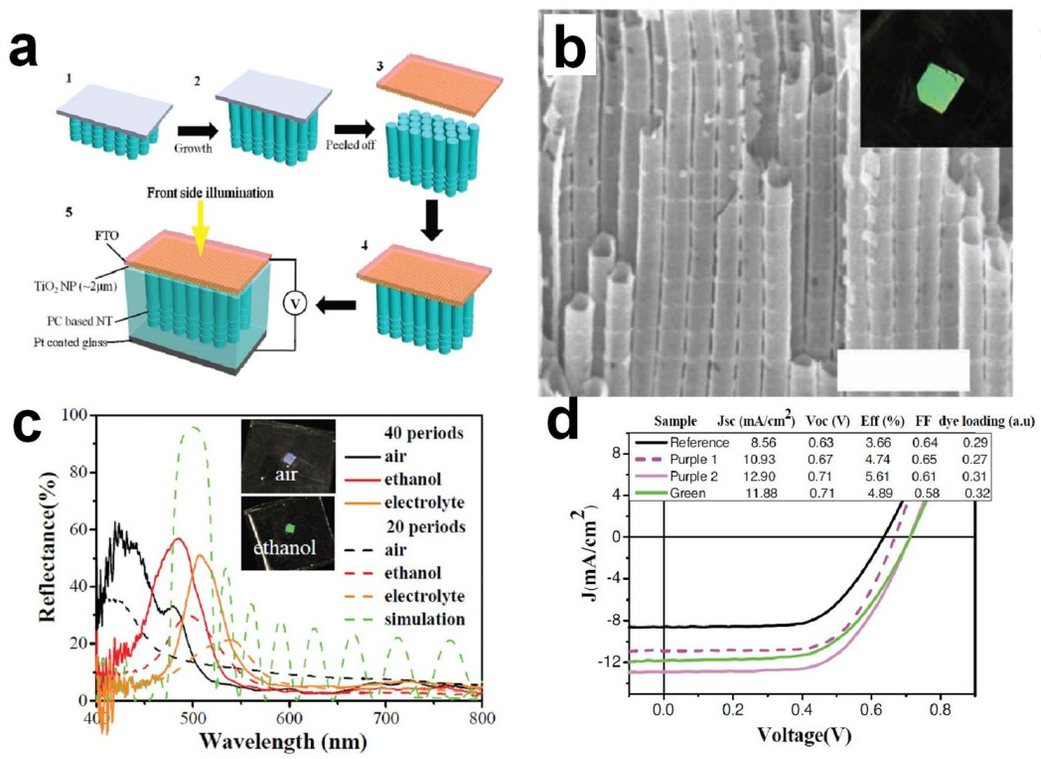


**Figure 23.** a) Schematic of the cell fabrication process. 1) Formation of PC layer. 2) Formation of NT layer. 3) Detachment of bi-layer from substrate. 4) Gluing to FTO by $TiO_2$ NPs. 5) Assembly of DSC. b) Cross-section SEM image of the PC layer. Scale bar:1 μ m. c) Reflectance of PC layers with 20 and 40 periods (lattice constant ~ 150 nm). Insets: photographs of the samples (with 20 periods) in air and infiltrated with ethanol. The green curves are simulated results with lattice constants of 150 and 190 nm for purple and green samples. d) *J*-V curves under AM 1.5 solar light illumination. The axial lattice parameters in the PC layer of the purple and green cells are ~ 150 and ~ 190 nm, and the numbers of periods are 30 and 20, respectively. Purple 1 and purple 2 are similar cells with a slight difference in dye loading. (Yip et al., 2012).

To solve a series of problems related to the PC coupled DSCs, including the poor physical contact between the PC layer and the $TiO_2$ absorbing layer, and the poor charge transport due to the nonconductive nature of PC, etc., C. T. Yip et al. developed a seamless PC-$TiO_2$ nanotube assembly (Yip et al., 2012), where the $TiO_2$ nanotube (NT) layer was fabricated by normal electrochemical anodization and the $TiO_2$ PC layer was obtained by a periodic current pulse anodization (Figure 23). Corresponding DSCs showed a 50% efficiency improvement compared with the cells without a PC layer, due to the enhanced light harvesting of the DSCs in the spectral range corresponding to the photonic bandgap of the PC and a longer wavelength range.

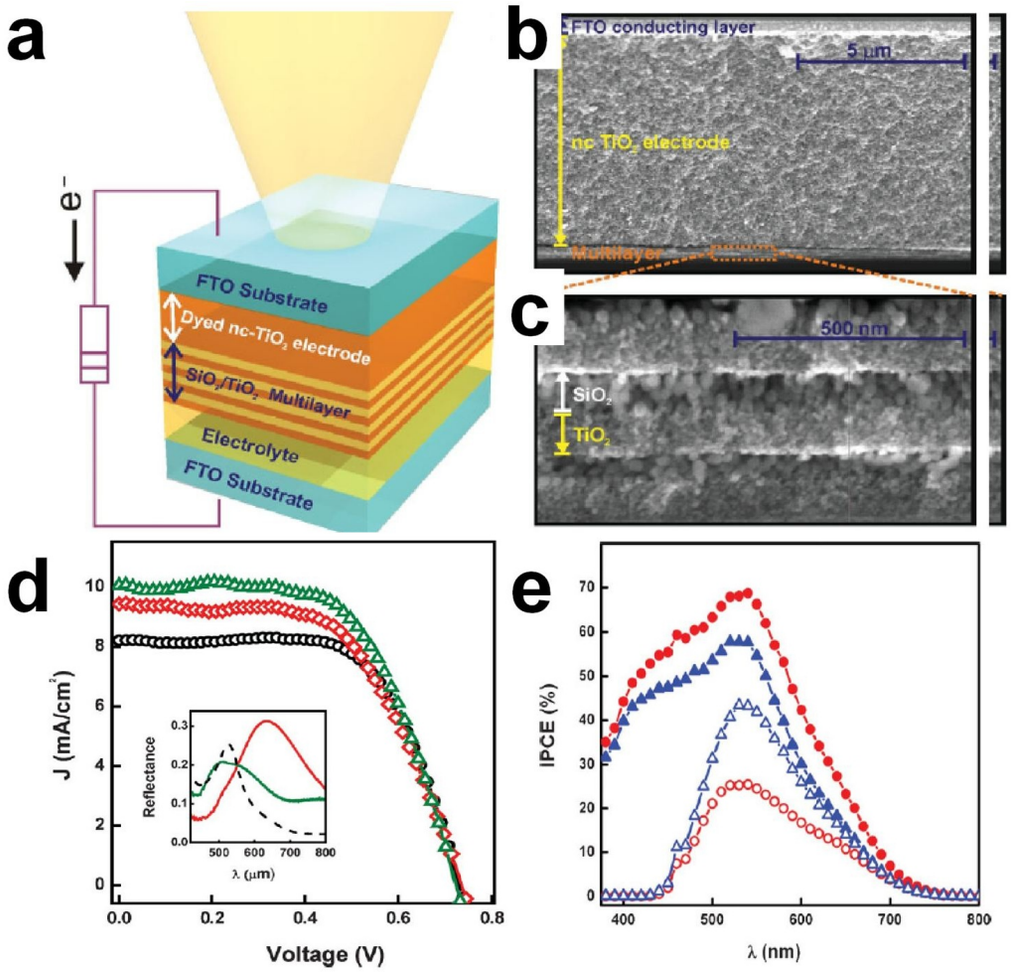


**Figure 24.** a) Scheme of DSC based on the 1D PC exposed to frontal illumination. b) Cross-section SEM image of nc-$TiO_2$ electrode, onto which a $TiO_2$–$SiO_2$ NP multilayer is deposited. c) Magnified view of the $SiO_2$ and $TiO_2$ layers composing the 1D PC. d) *J*–*V* curves of nc-$TiO_2$ electrode (7.5 mm thick) coupled to different 1D PCs under one-sun illumination. The lattice parameters are 120±10 nm (open green triangles), and 160±10nm (open red diamonds). Reference cell with the same nc-$TiO_2$ electrode is plotted as the open black circle line. Inset: reflectance spectra of the PC-based cell together with the absorption spectrum of the ruthenium dye. e) IPCE spectra for a DSC containing a 7.5 mm thick dye-sensitized $TiO_2$ electrode (solid blue triangles) and for the same electrode coupled to a PC of parameters 120±10nm (solid red circles), measured under frontal illumination and rear illumination (open blue triangles and open red circles, respectively). (Colodrero et al., 2009).

S. Colodrero, et al. couped a porous and highly reflecting 1D photonic crystal into a nc-$TiO_2$ electrode, by the deposition of alternate layers of NPs of different compositions by spin-coating (Colodrero et al., 2009). While the porous mesostructure allowed the electrolyte to flow through it and soak the electrode without interfering with the charge transport through the cell, the PC layer with a thickness of just half a micrometer efficiently localized the incident light within the nc-dyed $TiO_2$ electrode in a targeted wavelength range (Figure 24). Consequently, the average PCEs were improved to between 15 and 30% of the reference value attained for standard electrodes, while the open-circuit voltage and the transparency of the cell remained intact, contrary to what happened when the scattering layers were employed to improve the light harvesting.

http://dx.doi.org/10.5772/51633

Apart from the intensive studies on the PCs based DSC, other optical elements such as planar waveguide were also explored to enhance the LHE of DSC. Typically, Z. L. Wang's group demonstrated a novel three-dimensional DSC by integrating planar optical waveguide and nanowires (NWs) (Wei et al., 2010). The ZnO NWs were grown normally to the quartz slide, and the 3D cell was constructed by alternatively stacking a slide and a planar electrode. While the slide served as a planar waveguide for light propagation, the 3D structure effectively increased the light absorbing surface area due to internal multiple reflections without increasing the electron path length to the collecting electrode. Obtained 3D DSCs exhibited a significant improvement in energy conversion efficiency by a factor of 5.8 compared to the planar illumination case.

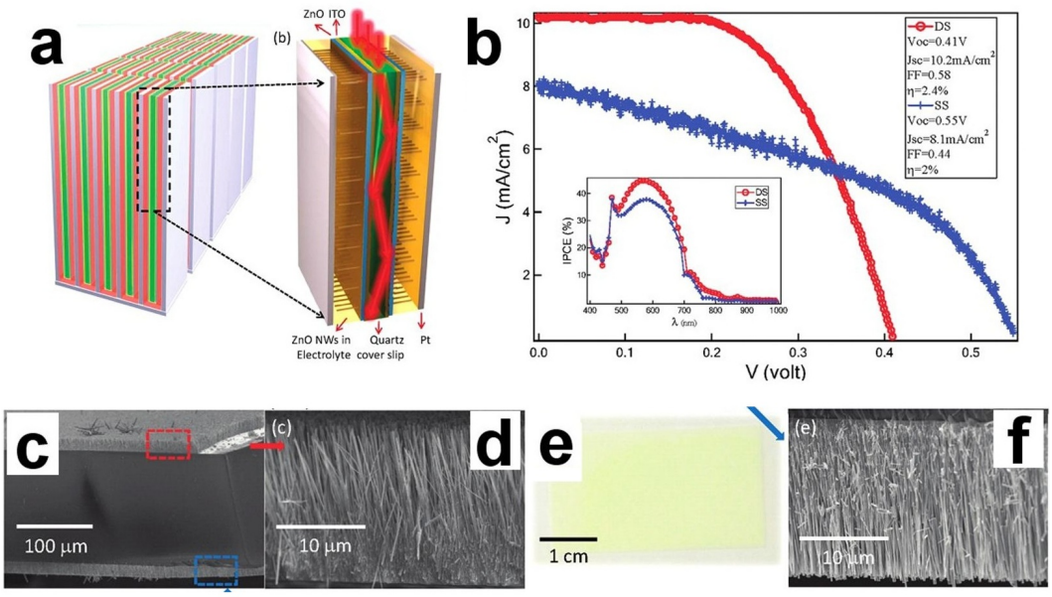


**Figure 25.** a) Schematic architecture of large scale 3D DSSC. The waveguide-NW 3D unit cells are plugged into the counter electrode housing and then sealed and fully packaged. b) *J*-V curves of DSCs under one full sun illumination for the parallell to the waveguide surface (PS) configuration. Inset: typical IPCE curves measured for single-side (SS) and double-side (DS) coated DSCs in the PS case. c) Low-magnification SEM image of a quartz slide with uniformly grown ZnO NWs on DS surfaces. d, f) High-magnification SEM images showing the densely packed ZnO NWs on top and bottom surfaces of the slide, respectively. e) Image of a slide coated with grown ZnO nanowire arrays. (Wei et al., 2010).

In summary, the optical elements such as the photonic crystals and the planar waveguide can provide exciting perspective to deliberately modulate the optical path of the incident lights and to significantly enhance the LHE of DSC. However, the ultimate PCE of corresponding DSCs is still far lower than that of nc-$TiO_2$ counterpart. How to tackle with the preparation problems related to the PC layers, and to avoid the possible adverse effects of the PC layers on the dye-loading and charge-transporting properties of the original electrode, are the kernel issues which should be solved in near future.

## 8. Conclusion

In conclusion, the light-harvesting efficiency (LHE) of the photoanode film has determinative effects on the power conversion efficiency of DSC. The deliberate modulations of the internal surface area of the nanoporous electrode and the optical path of the incident light are currently the main pathway to enhance the LHE of DSC. A wide range of novel materials or techniques have been utilized to improve the LHE of the electrode, including the high-surface area mesoporous nanostructures or aerogel, scattering-enhanced hierarchical nanostructures, up-conversion materials, plasmonic core-shell structures, and photonic crystals etc. However, while most of reported work realized obvious enhancement on one or more specific capacities of DSC, such as the dye-loading properties, optical scattering, or improved harvesting of near-infrared light, very few study can demonstrate high device performance comparable with the state-of-the-art nc-$TiO_2$ cell. The intrinsically different particle size, microstructures, preparation strategy of these novel materials from the traditional nc-$TiO_2$ electrode will inevitably result in significant changes in the microstructure or the optical/ electrical properties of the photoanode, which may greatly impair the final performance of the device. How to balance the advantageous and disadvantageous factors involved in these new-type photoanodes, and realize the solid improvement of the overall performance of DSC, are the emphasis of the scientists in near future. After all, the photoanodes based these novel materials or structures are still in an infant stage, containing infinite possibilities to improve or even revolutionize the basic principle and performance of the traditional DSC. We believe, via the intensive and extensive efforts of the scientist all over the world and through the collaborative studies among different areas spanning from material, chemistry to physics, the new-type photoanodes will certainly usher a brilliant future.

## Acknowledgements

This work is supported by the 973-project (Grant no. 2009CB623304) of Ministry of Science and Technology of China and the Basic Research Program (Grant no. 51072214, 51002174) of National Natural Science Foundation of China.

## Author details

Xiang-Dong Gao*, Xiao-Min Li and Xiao-Yan Gan

*Address all correspondence to: xdgao@mail.sic.ac.cn

State Key Lab of High Performance Ceramics and Superfine Microstructures, Shanghai Institute of Ceramics, Chinese Academy of Sciences, Shanghai, P. R. China

## References

[1] Brown, M. D., Suteewong, T., Kumar, R. S. S., Innocenzo, V. D., Petrozza, A., Lee, M. M., Wiesner, U., & Snaith, H. J. (2011). Plasmonic Dye-Sensitized Solar Cells Using Core–Shell Metal–Insulator Nanoparticles. *Nano Lett.*, 11(2), 438-445.

[2] Chen, W., Sun, X., Cai, Q., Weng, D., & Li, H. (2007). Facile Synthesis of Thick Ordered Mesoporous $TiO_2$ Film for Dye-Sensitized Solar Cell Use. *Electrochem. Comm.*, 9(3), 382-385.

[3] Chen, D, Huang, F, Cheng, Y. B., & Caruso, R. A. (2009). Mesoporous Anatase $TiO_2$ Beads with High Surface Areas and Controllable Pore Sizes: A Superior Candidate for High-Performance Dye-Sensitized Solar Cells. *Adv. Mater.*, 21(20), 2206-2210.

[4] Cho, C. Y., & Moon, J. H. (2011). Hierarchically Porous $TiO_2$ Electrodes Fabricated by Dual Templating Methods for Dye-Sensitized Solar Cells. *Adv. Mater.*, 23(26), 2971-2975.

[5] Choi, H., Chen, W. T., & Kamat, P. V. (2012). Know Thy Nano Neighbor. Plasmonic versus Electron Charging Effects of Metal Nanoparticles in Dye-Sensitized Solar Cells. *ACS Nano*, 6(5), 4418-4427.

[6] Colodrero, S., Mihi, A., Haggman, L., Ocana, M., Boschloo, G., Hagfeldt, A., & Miguez, H. (2009). Porous One-Dimensional Photonic Crystals Improve the Power-Conversion Efficiency of Dye-Sensitized Solar Cells. *Adv. Mater.*, 21(7), 764-770.

[7] Desilvestro, J., Grätzel, M., Kavan, L., Moser, J. E., & Augustynski, J. (1988). Highly Efficient Sensitization of Titanium Dioxide. *J. Am. Chem. Soc.*, 107(10), 2988-2990.

[8] Ding, I. K., Zhu, J., Cai, W., Moon, S. J., Cai, N., Wang, P., Zakeeruddin, S. M., Grätzel, M., Brongersma, M. L., Cui, Y., & Mc Gehee, M. D. (2011). Plasmonic Dye-Sensitized Solar Cells. *Adv. Energy Mater.*, 1(1), 52-57.

[9] Fan, K., Zhang, W., Peng, T., Chen, J., & Yang, F. (2011). Application of $TiO_2$ Fusiform Nanorods for Dye-Sensitized Solar Cells with Significantly Improved Efficiency. *J. Phys. Chem. C*, 115(34), 17213-17219.

[10] Ferber, J., & Luther, J. (1998). Computer Simulations of Light Scattering and Absorption in Dye-Sensitized Solar Cells. *Sol. Energy Mater. Sol. Cells*, 54(1-4), 265-275.

[11] Gaĺvez, F. E., Kemppainen, E., Míguez, H., & Halme, J. (2012). Effect of Diffuse Light Scattering Designs on the Efficiency of Dye Solar Cells: An Integral Optical and Electrical Description. *J. Phys. Chem. C*, 116(21), 11426-11433.

[12] Gao, X. D., Li, X. M., Gan, X. Y., Wu, Y. Q., Zheng, R. K., Wang, C. L., Gu, Z. Y., & He, P. (2012). Aerogel Based $SiO_2$-$TiO_2$ Hybrid Photoanodes for Enhanced Light Harvesting in Dye-Sensitized Solar Cells. *J. Mater. Chem.*, 22(36), 18930-18938.

[13] Gao, F., Wang, Y., Shi, D., Zhang, J., Wang, M. K., Jing, X. Y., Humphry-Baker, R., Wang, P., Zakeeruddin, S. M., & Grätzel, M. (2008). Enhance the Optical Absorptivity

of Nanocrystalline $TiO_2$ Film with High Molar Extinction Coefficient Ruthenium Sensitizers for High Performance Dye-Sensitized Solar Cells. *J. Am. Chem. Soc.*, 130(32), 10720-10728.

[14] Gratzel, M. (2009). Recent Advances in Sensitized Mesoscopic Solar Cells. *Acc. Chem. Res.*, 42(11), 1788-1798.

[15] Hagfeldt, A., Boschloo, G., Sun, L., Kloo, L., & Pettersson, H. (2010). Dye-Sensitized Solar Cells. *Chem. Rev.*, 110(11), 6595-6663.

[16] Hamann, T. W., Martinson, A. B. F., Elam, J. W., Pellin, M. J., & Hupp, J. T. (2008a). Aerogel Templated ZnO Dye-Sensitized Solar Cells. *Adv. Mater.*, 20(8), 1560-1564.

[17] Hamann, T. W., Martinson, A. B. F., Elam, J. W., Pellin, M. J., & Hupp, J. T. (2008b). Atomic Layer Deposition of $TiO_2$ on Aerogel Templates: New Photoanodes for Dye-Sensitized Solar Cells. *J. Phys. Chem. C*, 112(27), 10303-10307.

[18] Han, S. H., Lee, S., Shin, H., & Jung, H. S. (2011). Quasi-Inverse Opal Layer Based on Highly Crystalline $TiO_2$ Nanoparticles: A New Light-Scattering Layer in Dye-Sensitized Solar Cells. *Adv. Energy Mater.*, 1(4), 546-550.

[19] Hore, S., Vetter, C., Kern, R., Smit, H., & Hinsch, A. (2006). Influence of Scattering Layers on Efficiency of Dye-Sensitized Solar Cells. *Sol. Energy Mater. Sol. Cells*, 90(9), 1176-1188.

[20] Huang, F., Chen, D., Zhang, X. L., Caruso, R. A., & Cheng, Y. B. (2010). Dual-Function Scattering Layer of Submicrometer-Sized Mesoporous $TiO_2$ Beads for High-Efficiency Dye-Sensitized Solar Cells. *Adv. Funct. Mater.*, 20(8), 1301-1305.

[21] Huang, C. H., Yang, Y. T., & Doong, R. A. (2011). Microwave-Assisted Hydrothermal Synthesis of Mesoporous Anatase $TiO_2$ via Sol-Gel Process for Dye-Sensitized Solar Cells. *Microporous Meseporous Mater.*, 142(2-3), 473-480.

[22] Hüsing, N., & Schubert, U. (1998). Aerogels-Airy Materials: Chemistry, Structure, and Properties. *Angew. Chem. Int. Ed.*, 37(1-2), 22-45.

[23] Jeong, N. C., Prasittichai, C., & Hupp, J. T. (2011). Photocurrent Enhancement by Surface Plasmon Resonance of Silver Nanoparticles in Highly Porous Dye-Sensitized Solar Cells. *Langmuir*, 27(23), 14609-14614.

[24] Kim, J. Y., Kang, S. H., Kim, H. S., & Sung, Y. E. (2010). Preparation of Highly Ordered Mesoporous $Al_2O_3/TiO_2$ and Its Application in Dye-Sensitized Solar Cells. *Langmuir*, 26(4), 2864-2870.

[25] Ko, S. H., Lee, D., Kang, H. W., Nam, K. H., Yeo, J. Y., Hong, S. J., Grigoropoulos, C. P., & Sung, H. J. (2011). Nanoforest of Hydrothermally Grown Hierarchical ZnO Nanowires for a High Efficiency Dye-Sensitized Solar Cell. *Nano Lett.*, 11(2), 666-671.

[26] Koo, H. J., Kim, Y. J., Lee, Y. H., Lee, W. I., Kim, K., & Park, N. G. (2008). Nano-embossed Hollow Spherical $TiO_2$ as Bifunctional Material for High-Efficiency Dye-Sensitized Solar Cells. *Adv. Mater.*, 20(1), 195-199.

[27] Law, M., Greene, L. E., Johnson, J. C., Saykally, R., & Yang, P. (2005). Nanowire dye-sensitized solar cells. *Nature Materials*, 4(6), 455-459.

[28] Nazeeruddin, M. K., Kay, A., Rodicio, I., Humphry-Baker, R., Mueller, E., Liska, P., Vlachopoulos, N., & Grätzel, M. (1993). Conversion of Light to Electricity by Cis-X2bis(2,2′-bipyridyl-4,4′-dicarboxylate)ruthenium(II) Charge-Transfer Sensitizers (X = $Cl^-$, $Br^-$, $I^-$, $CN^-$, and $SCN^-$) on Nanocrystalline Titanium Dioxide Electrodes. *J. Am. Chem. Soc.*, 115(14), 6382-6390.

[29] Nazeeruddin, M. K., Pechy, P., Renouard, T., Zakeeruddin, S. M., Humphry-Baker, R., Comte, P., Liska, P., Cevey, L., Costa, E., Shklover, V., Spiccia, L., Deacon, G. B., Bignozzi, C. A., & Grätzel, M. (2001). Engineering of Efficient Panchromatic Sensitizers for Nanocrystalline $TiO_2$-Based Solar Cells. *J. Am. Chem. Soc.*, 123(8), 1613-1624.

[30] Regan, B. O., Moser, J., Anderson, M., & Grätzel, M. (1990). Vectorial Electron Injection into Transparent Semiconductor Membranes and Electric Field Effects on the Dynamics of Light-Induced Charge Separation. *J. Phys. Chem.*, 94(24), 8720-8726.

[31] Pietron, J. J., Stux, A. M., Compton, R. S., & Rolison, D. R. (2007). Dye-Sensitized Titania Aerogels as Photovoltaic Electrodes for Electrochemical Solar Cells. *Sol. Energy Mater. Sol. Cells*, 91(12), 1066-1074.

[32] Qi, J., Dang, X., Hammond, P. T., & Belcher, A. M. (2011). Highly Efficient Plasmon-Enhanced Dye-Sensitized Solar Cells through Metal@Oxide Core-Shell Nanostructure. *ACS Nano*, 5(9), 7108-7116.

[33] Qiu, J., Zhuge, F., Li, X., Gao, X., Gan, X., Li, L., Weng, B., Shi, Z., & Hwang, Y. H. (2012). Coaxial multi-shelled $TiO_2$ nanotube arrays for dye sensitized solar cells. J. Mater. Chem. , 22(8), 3549-3554.

[34] Regan, B. O., Moser, J., Anderson, M., & Grätzel, M. (1990). Vectorial Electron Injection into Transparent Semiconductor Membranes and Electric Field Effects on the Dynamics of Light-Induced Charge Separation. *J. Phys. Chem.*, 94(24), 8720-8726.

[35] Regan, B. O., & Grätzel, M. (1991). A Low-Cost, High-Efficiency Solar Cell Based on Dye-Sensitized Colloidal $TiO_2$ Films. *Nature*, 353(6346), 737-740.

[36] Sauvage, F., Chen, D., Comte, P., Huang, F., Heiniger, L. P., Cheng, Y. B., Caruso, R. A., & Gratzel, M. (2010a). Dye-Sensitized Solar Cells Employing a Single Film of Mesoporous $TiO_2$ Beads Achieve Power Conversion Efficiencies Over 10%. *ACS Nano*, 4(8), 4420-4425.

[37] Sauvage, F., Fonzo, F. D., Bassi, A. L., Casari, C. S., Russo, V., Divitini, G., Ducati, C., Bottani, C. E., Comte, P., & Graetzel, M. (2010b). Hierarchical $TiO_2$ Photoanode for Dye-Sensitized Solar Cells. *Nano Lett.*, 10(7), 2562-2567.

[38] Shan, G. B., Assaaoudi, H., & Demopoulos, G. P. (2011). Enhanced Performance of Dye-Sensitized Solar Cells by Utilizationofan External, Bifunctional Layer Consisting of Uniform β-$NaYF_4$:$Er^{3+}$/$Yb^{3+}$ Nanoplatelets. *ACS Appl. Mater. Interfaces*, 3(9), 3239-3243.

[39] Shao, F, Sun, J, Gao, L, Yang, S, & Luo, J. (2011). Template-Free Synthesis of Hierarchical $TiO_2$ Structures and Their Application in Dye-Sensitized Solar Cells. *ACS Appl. Mater. Interfaces*, 3(6), 2148-2153.

[40] Tetreault, N., & Grätzel, M. (2012). Novel Nanostructures for Next Generation Dye-Sensitized Solar Cells. *Energy Environ. Sci.*, 9(5), 8506-8516.

[41] Wei, Y, Xu, C, Xu, S, Li, C, Wu, W, & Wang, Z. L. (2010). Planar Waveguide−Nanowire Integrated Three-Dimensional Dye-Sensitized Solar Cells. *Nano Lett.*, 10(6), 2092-2096.

[42] Xu, F., Dai, M., Lu, Y., & Sun, L. (2010). Hierarchical ZnO Nanowire-Nanosheet Architectures for High Power Conversion Efficiency in Dye-Sensitized Solar Cells. *J. Phys. Chem. C*, 114(6), 2776-2782.

[43] Yella, A., Lee, H. W., Tsao, H. N., Yi, C., Chandiran, A. K., Nazeeruddin, M. K., Diau, E. W., Diau, G., Yeh, C. Y., Zakeeruddin, S. M., & Grätzel, M. (2011). Porphyrin-Sensitized Solar Cells with Cobalt (II/III)-Based Redox Electrolyte Exceed 12 Percent Efficiency. *Science*, 334(6056), 629-634.

[44] Yang, L., & Leung, W. W. F. (2011). Application of a Bilayer $TiO_2$ Nanofiber Photoanode for Optimization of Dye-Sensitized Solar Cells. *Adv. Mater.*, 23(39), 4559-4562.

[45] Yip, C. T., Huang, H., Zhou, L., Xie, K., Wang, Y., Feng, T., Li, J., & Tam, W. Y. (2012). Direct and Seamless Coupling of $TiO_2$ Nanotube Photonic Crystal to Dye-Sensitized Solar Cell: A Single-Step Approach. *Adv. Mater.*, 23(47), 5624-5628.

[46] Yum, J. H., Baranoff, E., Wenger, S., Nazeeruddin, M. K., & Grätzel, M. (2011). Panchromatic Engineering for Dye-Sensitized Solar Cells. *Energy Environ. Sci.*, 4(3), 842-857.

[47] Yun, T. K., Park, S. S., Kim, D., Hwang, Y. K., Huh, S., Bae, J. Y., & Won, Y. S. (2011). Pore-Size Effect on Photovoltaic Performance of Dye-Sensitized Solar Cells Composed of Mesoporous Anatase-Titania. *J. Power Sources*, 196(7), 3678-3682.

[48] Zhang, Q., & Cao, G. Z. (2011). Nanostructured photoelectrodes for dye-sensitized solar cells. *Nano Today*, 6(1), 91-109.

[49] Zhuge, F., Qiu, J., Li, X., Gao, X., Gan, X., & Yu, W. (2011). Toward Hierarchical $TiO_2$ nanotube Arrays for Efficient Dye-Sensitized Solar Cells. *Adv. Mater.*, 23(11), 1330-1334.